Preferred citation: W.W. Sampson. The Structural Characterisation of Fibre Networks in Papermaking Processes – A Review. In **The science of papermaking**, *Trans. of the XIIth Fund. Res. Symp. Oxford, 2001*, (C.F. Baker, ed.), pp 1205–1288, FRC, Manchester, 2018. DOI: 10.15376/frc.2001.2.1205.

THE STRUCTURAL CHARACTERISATION OF FIBRE NETWORKS IN PAPERMAKING PROCESSES – A REVIEW

W.W. Sampson

Department of Paper Science, UMIST,
PO Box 88, Manchester, M60 1QD, UK.
w.sampson@umist.ac.uk

ABSTRACT

The literature concerning the structure of two- and three-dimensional fibre networks is reviewed. Emphasis is placed on the literature concerning such networks in papermaking processes, though examples are drawn from other systems. The propensity of a suspension to flocculate is considered from a theoretical viewpoint. The experimental techniques and structural descriptors applied in the characterisation of fibre networks are discussed. Theoretical studies of random networks are presented along with their use as reference structures and comparison is made between the main techniques used in the structural characterisation of essentially two-dimensional networks such as paper. The relationships between the distributions of mass and voids are examined and the dependence of sheet nonuniformity on that of the suspension from which it is formed is reviewed.

OUTLINE

INTRODUCTION

The process of papermaking is one of handling fibre networks and modifying their properties. These networks may be at low mass concentrations for certain operations such as screening and cleaning, and may be thickened to higher concentrations in, for example deinking processes. Ultimately, on delivery from the headbox to the papermachine a well mixed, low consistency, three dimensional suspension is thickened to form an essentially planar structure. The structure of these suspensions, that of the formed sheet, and the relationships between them is the subject of this review. Although chemical and mineral additives are present in most papermaking furnishes, we shall consider primarily the structure of *fibre* networks and not the influence of system chemistry on, for example, the agglomeration of fillers, which was recently reviewed in these symposia [1].

Naturally, in order to discuss the structure of fibre networks, we must consider the techniques used to quantify these structures. This document therefore discusses the techniques used to characterise fibre networks in suspension and in the sheet. Given these techniques, we examine the properties of idealised structures for fibre networks, namely 3D and 2D random fibre networks; the importance of such structures being that they allow the measurements made on real structures to be compared with a reference. We shall consider also the relationships between the structural characteristics of a planar network and those of the suspension from which it is formed. Certain structural characteristics of fibre networks are deterministically intractable and experimentally hard to measure; some workers have used simulation studies and these are discussed where appropriate.

FLOCCULATION PROPENSITY

On preliminary inspection, it is immediately apparent that the structure of a suspension of fibres at any consistency used in a typical papermaking process is nonuniform. The nonuniformity of the suspension arises in part because of the discontinuity between the solid fibres and the liquid suspending medium, which is typically water. Of more interest is the spatial nonuniformity of the network; this being primarily a consequence of fibre interactions whilst in motion resulting in agglomeration or *flocculation*. Kerekes *et al*. [2] note that the term flocculation describes both the state of a suspension and the process by which it arrives at that state and define a floc as a region of higher density than the average of the network.

We expect flocculation to be a dynamic process, with some fibres or groups of fibres leaving a given floc as others are incorporated; the relative rates of

these processes determining whether a system tends to a more flocculated or more disperse state. The propensity of a floc to disperse under some force is dependent on its structure, through the number of inter-fibre contacts in a floc, and on the nature of the cohesive forces occurring at these points of contact. Kerekes *et al*. [2] identify four classes of cohesive force which may occur at fibre-fibre contacts.

Colloidal Electrostatic and electrokinetic forces acting between small particles. The magnitude of such forces is dependent on the quality of contact, through surface roughness, and the presence of charge altering chemicals, *e.g*. retention aids.

Mechanical surface linkage When a force is applied to a given fibre in a network, motion relative to other fibres is opposed by a reactive force at points of contact due to mechanical entanglement or 'hooking'. Such hooking forces may occur for entanglement of fibres due to contortion, *e.g*. curl or kinking, or of surface fibrils.

Elastic Fibre Bending Fibres are restrained from straightening by contact with other fibres in the network resulting in normal forces due to friction at fibre contact points. Restraint is due to internal fibre stresses and requires at least three contacts per fibre.

Surface Tension By definition, such forces require undissolved gas to be present at points of fibre contact.

Flocculation is typically the predominant cause of nonuniformity in papermaking suspensions and the formed sheet. Nevertheless, two further effects are often given greater precedence in the specifications of paper products, these being in-plane anisotropy[1] and sheet two-sidedness. The fibre orientation distribution results from oriented flows and jet-to-wire speed difference in the forming section and is discussed in detail by Niskanen [4, 5] who notes also that there may be a secondary orientation effect caused by mechanical deformation of the wet web under strain. Two-sidedness of the sheet is much less of an issue for twin-wire formers than for Fourdriniers; the phenomenon is usually associated with a *z*-directional distribution of fines or fillers [6] and as such we will not examine it further.

For fibres in suspension to flocculate they must, of course, interact. A *critical concentration* was defined by Mason [7] as that where the expected

[1]In-plane anisotropy is usually specified in terms of, *e.g*. MD:CD tensile index ratio. Such properties are affected by the in-plane fibre orientation distribution *and* the differing degrees of shrinkage in the MD and CD due to restraint in the dryer section. See *e.g*. [3].

number of fibres in a sphere of diameter one mean fibre length is one. It follows directly from the definition of consistency that this concentration is given by

$$C_v^{crit} = \frac{3}{2A^2} \tag{1}$$

$$C_m^{crit} = \frac{6}{\pi}\frac{\delta}{\bar{\lambda}^2} \tag{2}$$

where C_v^{crit} is the dimensionless critical volumetric consistency; C_m^{crit} is the critical mass consistency ($kg\ m^{-3}$); A is the fibre aspect ratio given by the ratio of length to diameter; $\bar{\lambda}$ is the mean fibre length and δ is the mean fibre coarseness ($kg\ m^{-1}$). Kerekes *et al*. [2] note that for flexible fibres the effective mean fibre length is reduced and Equations (1) and (2) will therefore underestimate the critical consistency.

The concept of a critical consistency provides the basis for the *crowding factor* or *crowding number* introduced by Kerekes *et al*. in [2] and subsequently developed by Kerekes and Schell [8, 9]. The crowding number, n_{crowd} is defined as the expected number of fibres in a sphere of diameter one mean fibre length and is given by

$$n_{crowd} = \frac{2}{3}A^2 C_v \tag{3}$$

$$= \frac{\pi}{6}\frac{\bar{\lambda}^2}{\delta}C_m \tag{4}$$

$$\approx \frac{\bar{\lambda}^2}{2\delta}C_m \tag{5}$$

where C_v is the dimensionless volumetric fibre consistency and C_m is the mass consistency ($kg\ m^{-3}$). We note that when $C_v = C_v^{crit}$ and when $C_m = C_m^{crit}$, $n_{crowd} = 1$. Photographs taken within a fibre suspension containing a few percent dyed fibres are shown in Figure 1; simulated three dimensional structures and their associated projections are illustrated in Figure 2.

Recently, Kropholler and Sampson [10] considered the influence of a fibre length distribution on the crowding number. For a lognormal distribution of fibre lengths, which is typical of many papermaking systems [11, 12, 13], Kropholler and Sampson showed that the mean crowding number $\underline{n^*}_{crowd}$ was greater than that given by Equations (3) and (4) by a

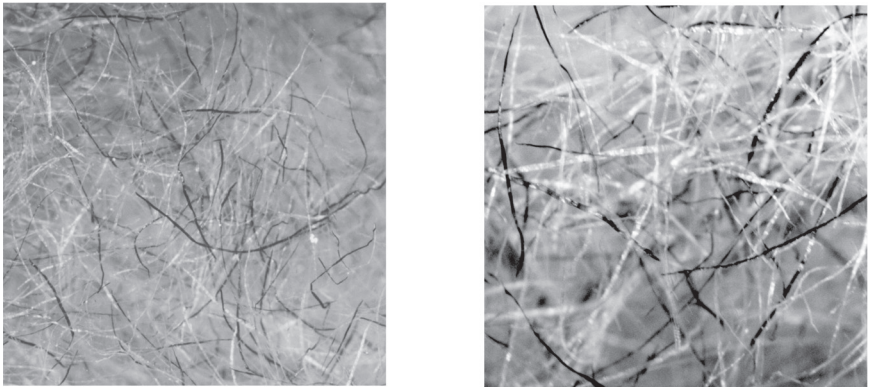

Figure 1 Photographs taken from within dilute fibre suspensions containing a few percent dyed fibres. Left: approx 8 *mm* × 8 *mm*; right: approx 4 *mm* × 4 *mm*. The pulp was a bleached kraft pine with a mean fibre length of around 2.5 *mm* at a mean consistency of around 0.1 %.

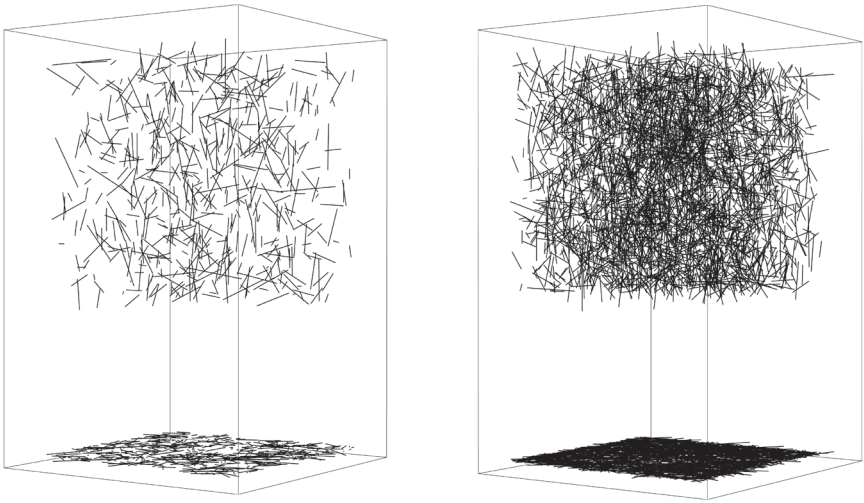

Figure 2 Simulated fibre suspensions. Lognormal distribution of fibre lengths with mean fibre length 1 *mm* and coefficient of variation 50 %; fibre coarseness 3×10^{-4} *g mm*$^{-1}$; volume represented is a cube of side 1 *cm*. Left: $C_m = 0.017$ %; right $C_m = 0.1$ %. Projections onto a plane are shown beneath each suspension.

factor depending only on the coefficient of variation of fibre length $CV(\lambda)$ such that

$$\overline{n^*}_{crowd} = n_{crowd}(1 + CV^2(\lambda))^4. \tag{6}$$

The dependence of the mean crowding number on the coefficient of variation of fibre length is very strong; a coefficient of variation of 50 % increasing the mean crowding number by around 2.4 times when compared to Equations (3) and (4).

Soszynski [14] investigated the relationship between the mass and volume consistencies of wood pulp suspensions. Denoting by w_k the Water Retention Ratio for fibres with walls at saturation point and lumens filled with water, the volumetric consistency is given by

$$C_v = \frac{\rho_w + \rho_{fib} w_k}{\rho_w + \rho_{fib}\left(\dfrac{1}{C_m} - 1\right)}, \tag{7}$$

where ρ_w and ρ_{fib} are the densities of water and dry fibre wall material respectively ($kg\ m^{-3}$). For C_m less than about 5 % and assuming $\rho_{fib} = 3\rho_w/2$ as is typical, we have the approximate relationship

$$C_v \approx \left(\frac{2}{3} + w_k\right) C_m \tag{8}$$

Sozynski reports values of C_v between 1.5 and 2.7 times those of C_m; absolute values depending on pulp type and drying history. Note also that the swelling of fibres in water reduces their aspect ratio A; the length of a dry fibre being similar to that of a wet fibre whereas swelling increases fibre width.

We shall see that correlations exist between the indices used to quantify flocculation in a given suspension and those used to quantify flocculation in a near-planar network formed from that suspension by a filtration type process. Before considering such relationships however, preliminary discussion will be given to the techniques used by researchers to quantify nonuniformity in fibre suspensions and in planar fibre networks.

MEASUREMENTS OF SUSPENSION STRUCTURE

When observing a fibre suspension, either in a static or dynamic state, the local consistency of the suspension is typically measured indirectly via an

optical technique using reflected or transmitted light. Measurements are usually made of a flowing suspension in a Plexiglas tube or channel as part of a flow loop. For 1D scans, as used for example by Wågberg [16] and Kaji and Monma [17], the light source is typically a monochromatic laser and the detector a photodiode.

Norman *et al*. [18] note that for low fibre concentrations illuminated by monochromatic light, the Beer-Lambert law for light transmission, given by Equation (9), applies and the transmittance decreases with increasing consistency and path length.

$$\tilde{I}(z) = \tilde{I}_0 e^{-\kappa \tilde{C}_m L} \tag{9}$$

where $\tilde{I}(z)$ is the local intensity of transmitted light through the suspension; $\tilde{I}_0$ is the local intensity of transmitted light with no fibres; κ is an absorption coefficient ($m^2\ kg^{-1}$); $\tilde{C}_m$ is the local mass consistency of the suspension ($kg\ m^{-3}$) and L is the path length of light through the sample (m).

In the same article, Norman *et al*. discuss the use of a fibre optic reflectance probe which is placed in a flowing suspension, full details of the technique are given in [24]. At consistencies above around 1 %, both transmission and reflectance techniques are subject to error due to secondary scattering effects. The reflectance technique has the disadvantage that flow is disrupted to some extent by the presence of the probe in the suspension, whereas the transmission technique can only yield information on the total mass concentration between the light source and the detector.

With the development of reliable CCD technologies, transmitted light measurements are increasingly carried out for 2D projections of fibre suspensions and image analysis. Kaji and Monma [17] used two lamps to illuminate the suspension, and compensated for nonuniform illumination by performing analysis on only the central region of the image where the light source was most uniform. The same approach was used by Beghello *et al*. [19] though the suspension was illuminated using either an electronic flash or a stroboscope depending on the flow velocity. More recently, Karema *et al*. [20, 21] used a DC regulated plane light source and compensated for nonuniform illumination by using the Beer-Lambert law to back-calculate the local intensity of incident light from the average of typically 200 images.

Characterising statistics

One of the simplest measures of flocculation calculated from the data obtained from experiments such as those discussed above is the coefficient of variation of local consistency, $CV\,(C_m)$ which is given by

$$CV_x(C_m) = \frac{\sigma_x(\tilde{C}_m)}{\overline{C_m}} \tag{10}$$

where $\sigma_x(\tilde{C}_m)$ is the standard deviation of local mass consistency at zone size x and $\overline{C_m}$ is the mean mass consistency. The standard deviation of local consistency will be dependent to some extent on the resolution of the sensors, and accordingly these should be quoted in the reporting of results. Wahren [15] classified this coefficient of variation as the *intensity of flocculation* by analogy to relative intensity of turbulence. The statistic was calculated by Kaji and Monma [17] for 1D data, but may be applied also to 2D data. For their 2D data, Kaji and Monma [17] calculated instead the fractal dimension of flocs in their images. This statistic was determined by thresholding images at the average grey level and creating a binary image of the network and rejecting small scale information. Fractal objects exhibit a scale invariance, such that

$$A_{floc}^{\frac{1}{2}} \propto P_{floc}^{\frac{1}{D_{frac}}} \tag{11}$$

where A_{floc} is floc area, P_{floc} is floc perimeter and D_{frac} is the fractal dimension. Thus, for a system exhibiting the scale invariance of fractals, a plot of log (A_{floc}) against log(P_{floc}) is linear with slope $2/D_{frac}$. Kaji and Monma [17] observed this linearity for their fibre suspensions and proposed that the fractal dimension was valid for flocs of area between 1 mm^2 to 300 mm^2; it was noted also that the shape index given by Equation (12) was inappropriate to characterise flocculated fibre networks as its value increased with increasing floc area.

$$Shape\ Index = \frac{P_{floc}^2}{4\pi A_{floc}} \tag{12}$$

Deng and Dodson [12] point out that the proportionality given in Equation (11) is expected for a 2D projection of a spherical floc; the fractal dimension having unit value. However, the shape index given by Equation (12) for such flocs also has unit value and is independent of floc area; note also that Kaji and Monma [17] observed values of D_{frac} of around 1.3.

The use of the *Power Spectrum* to characterise the state of flocculation in fibre networks again follows from its application in turbulence research. The technique was introduced by Norman and Wahren [22] for quantification of flocculation and turbulence in suspension and the distribution of mass density in sheets; we shall return to the application of the power spectrum to

formed sheets in the sequel. The technique uses Fourier analysis of the autocovariance of normally distributed data to partition the total variance within the data into components attributable to different scales of variability [12, 22, 23]. The full mathematical treatment applied by Norman and Wahren is given in [22]. Much of their early work used analogue signals, though digital processing is now typical; accordingly the general treatment of Dodson [12] is given here.

The *autocorrelation* of a stationary stochastic process, $c(t)$ is defined as the expected value of the product of the variable taken over all points separated by a distance, τ and is given by

$$\mathcal{R}(\tau) = E\{c(t)\,c(t+\tau)\}, \tag{13}$$

and the *autocovariance* of $c(t)$ is given by

$$\mathcal{C}(\tau) = \mathcal{R}(\tau) - \overline{c(t)}^2, \tag{14}$$

where $\overline{c(t)}$ is the mean value of the stochastic variable and $\mathcal{C}(0)$ is the variance of $c(t)$. The Fourier transform of the autocovariance is

$$\mathcal{P}(\upsilon) = 2\int_0^\infty \mathcal{C}(\tau)\cos(2\pi\upsilon\tau).d\tau \tag{15}$$

and υ is the 'spatial frequency'.

Equation (15) gives the *frequency power spectrum* used by Norman and Wahren [22]; the stochastic variable of interest in their flocculation studies being the deviation of the local consistency from the mean normalised by the mean. Denoting 'spatial wavelength', l, such that $\upsilon l = \bar{v}$, the *wavelength power spectrum* is given by,

$$\mathcal{P}(l) = \frac{\bar{v}}{l^2}\mathcal{P}\left(\frac{\bar{v}}{l}\right). \tag{16}$$

In this form, the power spectrum is independent of the mean flow velocity $\bar{v}$ and the wavelength l corresponds to twice the geometrical size of flocs contributing to the variance [22, 24].

Dodson points out [12] that, as with the other techniques discussed, the resolution of the detector limits the amount of information obtained at the highest frequency. The variance contribution within a given wavelength band is determined by integration of the power spectrum between the lower and

upper bounds of a given band. Norman and Wahren [22] use the power spectrum to define also the characteristic lengths of variations such that the *micro-scale* is given by,

$$l_{micro}^2 = 8\pi^2 \frac{\int_0^\infty \mathcal{P}(\upsilon).d\upsilon}{\int_0^\infty \upsilon^2 \mathcal{P}(\upsilon).d\upsilon} \tag{17}$$

and l_{micro} provides a measure of the average size of variations. The *macro-scale* provides a measure of the size of the largest variations and is given by,

$$l_{macro} = \frac{\pi}{2} \frac{\mathcal{P}(0)}{\int_0^\infty \mathcal{P}(\upsilon) .\mathrm{d}\upsilon} \tag{18}$$

The power spectrum has been used extensively in the studies of Wågberg [25], who investigated principally chemically induced flocculation, and those of Beghello *et al*. [19, 26, 27] who defined a characteristic wavelength, l_{char} in the 2 *mm* to 32 *mm* range such that

$$\int_{2\,mm}^{l_{char}} \mathcal{P}(l).dl = \int_{l_{char}}^{32\,mm} \mathcal{P}(l) .dl \tag{19}$$

and the characteristic floc size, $FS_{char} = l_{char}/2$. Wågberg [25, 28] used wavelength power spectra for furnishes with and without flocculating polymers to characterise the degree of polymer-induced fibre flocculation by a flocculation index such that

$$F = \frac{\sqrt{V_a^2 - V_b^2}}{V_b} \tag{20}$$

where V_a and V_b are the coefficients of variation of their 1D data, for furnishes with and without polymer respectively.

MEASUREMENTS OF SHEET STRUCTURE

The measurements of network structure in suspension discussed above involved essentially quantification of the distribution of local consistency in the network. As the structure of fibre networks in suspension is unbonded and fibres are saturated with water, the relationships between consistency and porosity distribution are uncomplicated. The distributions of mass, voids and

density in the sheets formed from the filtration of suspensions have more complex inter-relationships; accordingly, here each is dealt with in turn.

Mass distribution

For sheets formed from undyed fibres at grammages of less than around 120 $g\ m^{-2}$, the degree of nonuniformity is immediately apparent on inspection of the sheet viewed under transmitted light. It is well established however that regions with a given local grammage may have different opacities; the difference arising from local differences in the degree of bonding, furnish, *etc*. and hence local light scattering coefficients. The relationship between local light transmittance and local grammage was discussed by Kommpa and coworkers [29, 30]; their equipment allowed simultaneous measurement of light transmission and β-ray absorption for 1 *mm* diameter circular zones. For unbeaten, lightly pressed and uncalendered sheets, the relationship between local grammage and local light transmission was approximately linear and hence agreement between the coefficients of variation was reasonable; however, the influence of beating, and more severe wet pressing and calendering operations is to reduce the scattering in the sheet and hence reduce also the coefficient of variation of local light transmission. Similar effects are reported by Bernié and Douglas [31], who classify highly scattering papers as "light transmission friendly". It is clear therefore that the use of light transmission techniques to infer mass distribution data, whilst suitable for fibres in suspension and lightly bonded networks, should be used with caution for most grades of paper. Typically, the distribution of mass in the plane of the sheet is of interest, since it is a direct consequence of the forming process; the distribution of optical density being determined by factors other than the process by which a network is formed.

The most direct measure of mass distribution in the plane of the sheet is the accurate weighing of small samples of precise and known area. Clearly such an activity is neither experimentally attractive, nor accurate at typical scales of interest. Consequently, several indirect radiographic techniques have been developed to measure local mass; the most widely used being contact β-radiography. Accordingly, here we consider the principles behind radiographic techniques and provide a more detailed discussion of the use of β-radiography.

Perhaps the earliest reference to the application of radiographic techniques to paper is given by Brazington and Radvan [32]. Samples of paper were held between an α-source, Polonium 210, and a photographic film. Through preliminary experiments exposing aluminium film in place of a paper sample, Brazington and Radvan determined that α-particles were prevented from

reaching the photographic film by approximately 37.7 $g\ m^{-2}$ of aluminium film, and that this corresponded to approximately 24 $g\ m^{-2}$ of cellulose; the two materials having differing rates of attenuation for α-radiation. By incorporating layers of different grammage of aluminium film between the source and the paper sheet, radiographs were obtained where exposed areas of the film represented areas of the sheet with grammage lower than a given value; the upper threshold for this value being 24 $g\ m^{-2}$.

The images presented by Brazington and Radvan [32] show clearly the grammage distribution which results from watermarking; wiremarks are also present, though it is not stated whether these arise from the forming fabric or the dandy roll. As a consequence of α-particles being essentially mono-energetic, the images are effectively binary. The authors note that there was some nonuniformity in the aluminium film, and in the distribution of radio-activity in the source; it is not possible therefore to identify any stochastic variability in the images obtained.

The technique of Brazington and Radvan [32] was used in a subsequent study by Parker and Attwood [33] who found that in a 50 $g\ m^{-2}$ newsprint sample, areas "the size of half-tone dots" were present with grammage less than 17 $g\ m^{-2}$. The study, along with a subsequent article by the same authors [34] concerns primarily the measurement of periodic variations in sheet grammage arising from the structure of the forming fabric; the import-ance of the work here is the use of contact β-radiography to investigate the grammage distribution in the plane of the sheet. Details of the experimental procedure used are sparse, but the fundamentals of the technique are those used by most researchers investigating paper structure today. The influence of several experimental variables has been discussed by Cresson *et al*. [35] and reasonably up-to-date methods of data acquisition are described by Ng [36]. Here a typical schema for the preparation and analysis of a β-radiograph from a paper sample is given.

A paper sample, of mean basis weight less than approximately 150 $g\,m^{-2}$ [37], is placed on a ^{14}C labelled Polymethyl Methacrylate sheet; at UMIST we use a 10 $cm \times 10\ cm \times 1\ mm$ sheet of specific activity, 1.48 $mCi\ g^{-1}$ and total activity 17.6 *mCi*. The paper sample covers a rectangle of approximately 8.5 $cm \times 10\ cm$ and the remainder of the β-source is covered with a mylar step wedge for grammage calibration; aluminium film has been used success-fully by some workers [33, 34]. The paper and mylar are covered with an X-ray photographic film and the layers are clamped between foam backed hard plates to ensure close contact. After a given time, previously determined to give good exposure, the sample is unclamped and the film developed and fixed; the resulting image on the X-ray film is a negative of the mass distribu-tion in the sheet. The optical densities of the exposed film in the region of the

calibration wedge are used to convert the optical densities in the region of the sheet into a mass distribution map. This was originally carried out using a densitometer [33, 34, 38, 39]; subsequently digital cameras and image-analysis procedures have been applied [36] and it is now standard practice to use a high-resolution computer scanner with an overhead transparency unit; the use of such a system for obtaining light transmission images is discussed by Enomae and Kuga [40]. The attenuation of β-rays by the sheet follows the Beer-Lambert law given in Equation (9) for the attenuation of light, such that

$$\tilde{I}(\tilde{\beta}) = I_0 \, e^{-\kappa' \tilde{\beta}}$$

where $\tilde{I}(\tilde{\beta})$ is the local intensity of attenuated β-rays; I_0 is the incident β-ray intensity, which may be assumed uniform; κ' is the mass absorption coefficient ($m^2 \, g^{-1}$) and $\tilde{\beta}$ is the local grammage ($g \, m^{-2}$).

Cresson *et al*. [35] investigated the influence of experimental variables such as film type, exposure time, developing time and temperature, *etc*. as well as image capture variables such as lens aperture and light intensity on the range and resolution of grammage measurements. Their results show the absorption coefficient, κ' to be very similar for mylar and paper and around 0.03 $m^2 \, g^{-1}$ for their most sensitive film, which was comparable to that obtained by other workers. For a given film type, Cresson *et al*. recommend that, in particular, the temperature and concentration of the developing fluid, and the developing time are held constant for a given study. A correctly exposed film has a characteristic S-shaped curve when the grey-level of the calibration wedges is plotted against their grammage; the basis weight range of the sheet should fall predominantly in the steepest region of the curve.

Recently, a β-radiographic system has been described by Keller and Pawlak [41] where the X-ray film is replaced by a storage phosphor system, greatly simplifying experimental procedures. The system is compared with standard β-radiography in [42].

The technique of β-transmission is the direct analysis of the attenuation of β-rays by paper via a scintillation counter. Instruments designed to measure local mass using β-transmission are described by Herdman and Corte [43], Komppa and Ebeling [29] and Waterhouse [44]; the technique has been applied in commercial formation sensors such as the Ambertec, see *e.g*. [45]; measurements are typically made on 1 *mm* diameter circular zones.

β-radiography is a time-consuming process and the typically used ^{14}C source is suitable only for sheets of mean grammage less than around 150 $g \, m^{-2}$ [37]. Electrography has been used by Tomimasu *et al*. [46] and is suitable for sheets of mean grammage up to 400 $g \, m^{-2}$ and provides higher resolution images. Another technique used for higher basis weight sheets is

soft X-radiography [37,47,48]. The techniques are compared for imaging newsprint by Tomimasu *et al*. [37] who found that β-radiography and electrography gave similar performance, the primary advantage of electrography being the speed with which an image may be acquired and a slightly higher spatial resolution. For good basis weight calibration, low energy soft X-rays should be used, and a shading correction applied to the image to overcome the 'heel effect' described by Farrington [48]; this being a geometrical effect caused by the angle of the target and imaging area. However, scattering within the sheet is minimal where soft X-rays are used, and consequently the spatial resolution is improved.

Characterising statistics

As with the quantification of nonuniformity in fibre suspensions, one of the most widely used descriptors is the coefficient of variation of local grammage at a given inspection zone size which is given by

$$CV_x(\tilde{\beta}) = \frac{\sigma_x(\tilde{\beta})}{\bar{\beta}}, \tag{21}$$

where $\sigma_x(\tilde{\beta})$ is the standard deviation of local grammage at zone size x and $\bar{\beta}$ is the mean sheet grammage. Of interest also is how the variance, standard deviation and hence coefficient of variation of local grammage are affected by the size of the zones we chose to inspect. Rather than acquiring images at different resolutions, averaging is typically carried out for $n \times n$ pixels and variance statistics calculated.

An alternative formation index, denoted the *specific formation* by Niskanen *et al*. [5] and the *normalised standard deviation* by Kajanto *et al*. [23], is given by

$$f_n = \frac{\sigma_x(\tilde{\beta})}{\sqrt{\bar{\beta}}}, \tag{22}$$

$$= \sqrt{\bar{\beta}}\, CV_x(\tilde{\beta}). \tag{23}$$

The index has dimensions of $g^{\frac{1}{2}}\, m$ and its definition probably arises from the property of a point Poisson process that $\sigma_x^2(\tilde{\beta}) = (\bar{\beta})$ and therefore for a random process, $f_n = 1$.

The power spectrum, as described earlier for the study of flocculation in fibre suspensions and given by Equations (15) and (16), may be used also to describe flocculation in sheets [22]; the stochastic variable $c(t)$ in

Equations (13) and (14) being the deviation of the local grammage of a zone from the mean, *i.e.* $\tilde{\beta} - \bar{\beta}$.

The power spectrum represents the contribution of flocs of different sizes to the overall variability in the sheet, as does a plot of variance, or coefficient of variation, of local grammage against zone size. This is illustrated via Figures 3 to 7.

Figure 3 shows 5 *cm* × 5 *cm* grammage maps of two paper samples with differing formation along with their power spectra and plots of the normalised variance against inspection zone size. It is immediately apparent from the plot of normalised variance against zone size that Sample 1 exhibits a higher variance of local grammage at all scales of inspection. The power spectrum for Sample 2 lies above that for Sample 1 at low wavelengths and *vice versa* at higher wavelengths, indicating that more of the variability in Sample 2 is due

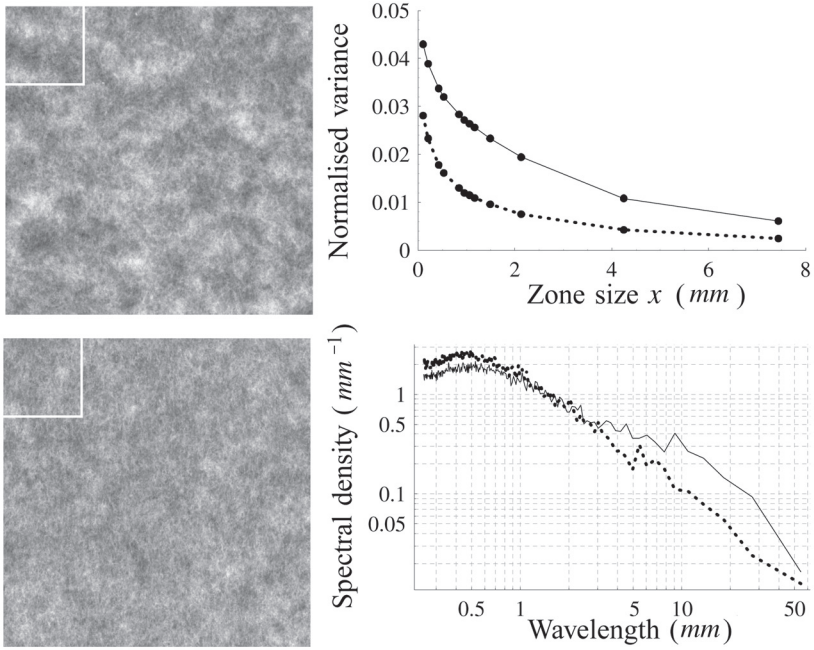

Figure 3 Comparison of Power Spectrum and variance against zone size. Top left: grammage map for Sample 1; bottom left: grammage map for Sample 2. Top right: normalised variance of local grammage plotted against inspection zone size; bottom right: power spectra. Sample 1: solid lines; Sample 2: broken lines.

to small scale flocs. Of course, for these samples these conclusions would be arrived at by simple visual inspection; note that the steeper decay of the variance against zone size plots at small scales of inspection of Sample 2 when compared to Sample 1 indicates also a small floc size.

Bandpass filtering has been applied to the Fourier transform of the grammage maps shown in Figure 3. It is typical in bandpass filtering to use circular regions; however, to recover the same information as shown in the variance against zone size plots, it is necessary to apply square filters[1]; for a recent thesis discussing the application of bandpass filtering to the analysis of print nonuniformity, see Johansson [49]. Also, these filters must be applied with the diagonals in the x and y directions, *i.e.* $\diamondsuit$ instead of $\square$ such that the wavelength bands correspond to $\sqrt{2}$ times the side of a square inspection zone; thus, whilst circular bands give an isotropic filter, here we have applied an orthotropic bandpass filter. Figures 4 and 5 show the grammage variations within given wavelength bands as determined by orthotropic bandpass filtering for Samples 1 and 2 respectively. The area represented in each plot is that marked by a white square in the top left hand corner of the grammage maps shown in Figure 3; the use of larger areas would mask the variability.

The normalised variances for the eight wavelength bands illustrated in Figures 4 and 5 are plotted in Figure 6. In agreement with the power spectra shown in Figure 3, it is clear that Sample 2 exhibits greater small scale variability than Sample 1 and *vice versa*. The same data are presented in cumulative form as points in Figure 7 where the abscissa represents the lower limit of the wavelength bands; the lines are the same as those in Figure 3, though the inspection zone sizes have been multiplied by 2 to be consistent with the sampling theory of Nyquist such that this is the minimum wavelength which may be sampled. A consequence of orthotropic bandpass filtering is that these wavelengths are correct in the x and y directions but will be longer by a factor up to $\sqrt{2}$ in all other directions. Figure 6 shows excellent agreement between the information contained in Power Spectra and that given in plots of variance against zone size.

Cresson and Luner [50] note that structural characterisation by second order statistics, *i.e.* variance and coefficient of variation, may not distinguish between structures with different textures; also, the power spectrum has been criticised as being difficult to interpret [50, 51]. The approach of Jordan and Nguyen and co-workers [51, 52, 53] has been to measure the *specific perimeter* of flocs in the sheet. This parameter is determined by thresholding a gram-

[1]In fact, there is an approximation in the use of square filters; the correct geometry is slightly more complex and will be discussed elsewhere.

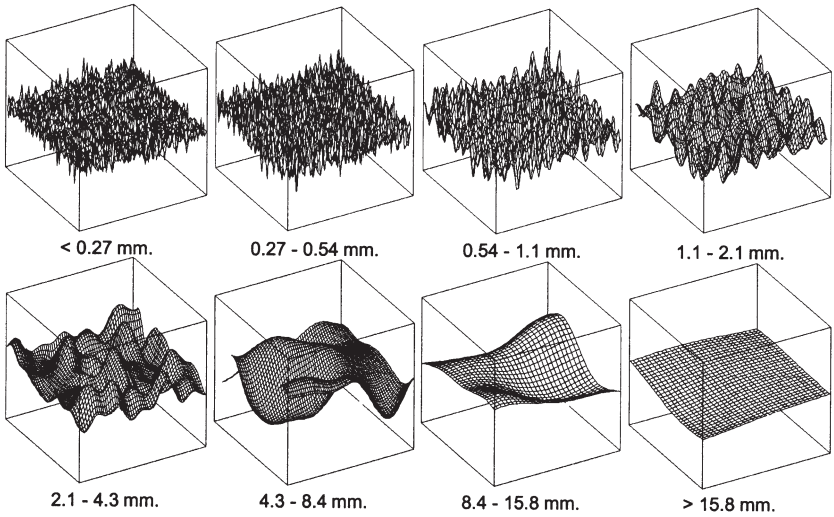

Figure 4 Grammage variations within given wavelength bands for Sample 1. Stated wavelengths apply to x and y directions only; full scale on vertical axis is 1 mean grammage.

mage map of the sheet at the median grammage and measuring the perimeter of all flocs not touching the edges of the measuring area. This value is weighted by the measuring area such that the specific perimeter is given by

$$P_{spec} = \frac{\sum_{i=1}^{n} P_{floc,i}}{A_{insp}} \tag{24}$$

where $P_{floc,i}$ is the perimeter of the ith object and n objects exist within a field of view with inspection area A_{insp}; the specific perimeter therefore has dimensions of reciprocal length. Jordan and Nguyen show in [51] that the specific perimeter is in fact related to the power spectrum such that

$$P_{spec}^2 = \frac{1}{4} \frac{\int_0^\infty \upsilon^2 \mathcal{P}(\upsilon) \, .d\upsilon}{\int_0^\infty \mathcal{P}(\upsilon) \, .d\upsilon}, \tag{25}$$

where $\mathcal{P}(\upsilon)$ is the frequency power spectrum given by Equation (15). The importance of this relationship is that the statistic may be computed from

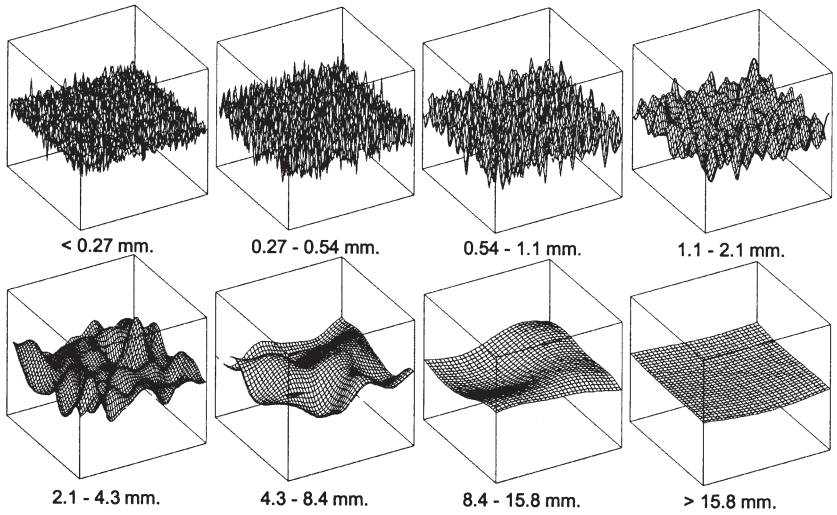

Figure 5 Grammage variations within given wavelength bands for Sample 2. Stated wavelengths apply to x and y directions only; full scale on vertical axis is 1 mean grammage.

line-scans and therefore might be applied in on-line formation instrumentation [51]. Comparison of Equation (25) with Equation (17) shows us that the specific perimeter and the micro-scale in fact quantify the same property of the power spectrum.

The *floc formation index* proposed by Bernié and Douglas [31] is given by,

$$FFI = \int_0^{\chi} \mathcal{P}(\upsilon)\ .d\upsilon \tag{26}$$

where χ is an arbitrary frequency quantifying the minimum size of flocs of interest in a given investigation.

Cresson and Luner [50] calculated texture-related descriptors from the co-occurrence matrix obtained from digitised contact β-radiographs; the algorithm used is described in [54]. The textural descriptors calculated were the energy, contrast, correlation, entropy and homogeneity. Cresson and Luner concluded however that such descriptors did not assess directly the structural properties of the sheet of interest to the papermaker. An alternative method of extracting data from texture maps was proposed in [55]; this involved the partitioning of the texture map at the median grammage and

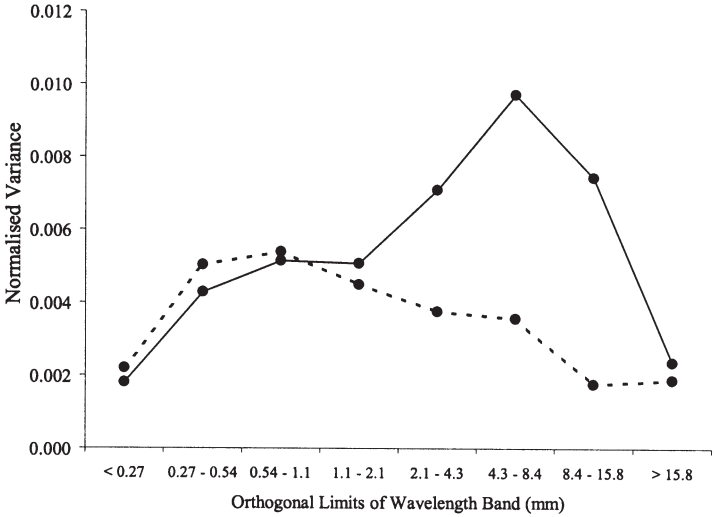

Figure 6 Normalised variance plotted for eight wavelength bands illustrated in Figures 4 and 5. Sample 1: solid lines; Sample 2: broken lines.

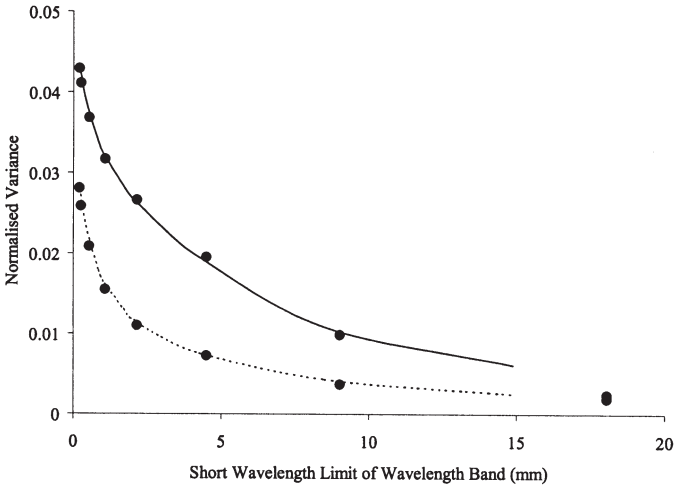

Figure 7 Cumulative normalised variance plotted against wavelength. Points determined by orthotropic bandpass filtering, lines are the same as those shown for variance against zone size in Figure 3. Sample 1: solid lines; Sample 2: broken lines.

quantifying the occurrence and dimensions of light and heavy zones. The statistics generated are related to those given by Kallmes and Ayer [57] who counted, and measured the areas and light transmission of, regions with light transmission less than the mean.

The wavelet transform has recently been applied to the characterisation of formation by Bouydain *et al*. [58] using light transmission images, and by Keller *et al*. for general classes of structures [59], and for simulated paper structures [60]. Keller *et al*. note that, for nonperiodic functions, the wavelet energy spectrum closely approximates the Fourier power spectrum; though the wavelet energy spectrum is better suited to the analysis of larger scale variations such as streaks and other CD and MD variations.

Void size distribution in sheets

The local porous structure of a fibre network is, by definition, the complement of its local mass structure. As such, we expect the distribution of fibres within the sheet to affect the distributions of porosity and the pore size distribution in the sheet.

Two experimental techniques still widely in use today were described by Corte [61]. Mercury *porosimetry* involves forcing mercury at increasing pressures into the sheet and recording the volume of mercury intruded at each pressure interval. The radius of pores entered at each pressure interval is given by the Kelvin equation:

$$r_p = -\frac{2\gamma}{p}\cos(\theta_c), \tag{27}$$

where r_p is the pore radius (m), γ is the surface tension ($N\,m$), p is the pressure ($N\,m^{-2}$) and θ_c is the contact angle between the mercury and the fibres. Corte assumed θ_c to be 180° such that $\cos(\theta_c) = -1$. Correction must be made for the compressibility of mercury at high pressures and care must be taken to ensure constant temperature of the system during experimentation. The technique gives the volume frequency pore radius distribution, *i.e*. the porous volume of the sheet associated with pores of given radii. The technique has been widely applied to the characterisation of the void structure of filled papers and paper coatings [62, 63] but has been applied to unfilled and uncoated sheets by Yamauchi and Kibblewhite [64, 65] who assumed $\theta_c = 140°$. Yamauchi and Kibblewhite define also an *apparent breakthrough pressure* which occurs at the maximum rate of intrusion of mercury into the voids and may be associated with mercury passing through small voids into larger spaces.

The second technique described by Corte [61] involves saturating the sample with a non-swelling fluid and displacing the fluid from the voids using dry nitrogen at increasing pressures. The output is a curve of flow rate against pressure from which the pore size distribution of an equivalent system of straight parallel and circular capillaries may be determined; an important difference between this technique, known as *porometry*, and mercury porosimetry is that the frequencies of pore radii are characterised by their number and not their volume. The technique and associated theory is described in detail in [66]. Despite the assumption of such a uniform geometry and the neglection of effects such as tortuosity and interconnectedness of voids, we shall see that the outputs from such flow based porometry experiments give excellent agreement with theories based on geometry.

Thickness and density variations

The thickness, and hence the density, of paper is notoriously difficult to measure accurately due to the nonuniform and compressible nature of the sheet. A study of the measurement techniques for mean sheet thickness was presented by Yamauchi [67] who compared the standard technique of measuring the separation of parallel hard circular platens applied around a sheet or stack of sheets at a standard load and standard rate of loading, with mercury buoyancy and pyncnometric techniques and with a modified platen technique using soft rubber platens, as developed by Wink and Baum [68]. The highest values were obtained using the standard technique, where the thickest regions of the sheet only are measured; values obtained using the soft platens, which conform to some extent to the sheet surface, were lower; the mercury techniques, where mercury covers the sheet surface well but does not penetrate into the bulk, gave markedly lower values.

An alternative measure of mean thickness, based on the mechanical properties of the sheet was proposed by Setterholm [69], such that

$$z_{eff} = \sqrt{\frac{12\,S}{E}}, \tag{28}$$

where z_{eff} is the effective thickness (m), S is the bending stiffness ($N\,m$) and E is the tensile stiffness ($N\,m^{-1}$).

Whilst such techniques allow determination of a mean thickness under a given set of conditions, they provide no information on its distribution. A technique for measuring the thickness of small zones was presented by Schultz-Ekland *et al.* [70]. The technique used a pair of small diameter

mutually opposing spherical platens to scan a square area of side 77 *mm*. In conjunction with β-radiographic measurements of local grammage for the same areas, Schultz-Ekland *et al*. produced thickness and grammage maps for calendered and uncalendered samples and determined the coefficients of variation of thickness, grammage and density at the 150 μm scale. Whilst the correlation between local grammage and local thickness was good, the measurement of thickness used a direct contact technique, and absolute values showed some sensitivity to platen diameter and measuring force. More recently, Izumi and Yoshida [71] have developed a non-contact method to measure a thickness distribution map using two-sided laser triangulation techniques.

MODELLING 3D NETWORKS

The flow behaviour of fibre suspensions is affected by flow conditions characterised by, *e.g*. the Reynolds Number, and the friction loss for flowing fibre suspensions differs from that observed for water [18]. Turbulent energy from the fluid serves to disrupt the fibre network in suspension and hence influences network structure. Conversely, in decaying turbulence, the network structure becomes more coherent [72]. Models of the network structure in three dimensions, coupled with those describing structure in two dimensions and appropriate experiments, provide insights into the relationships between sheet and suspension structure. Here, we consider first the properties of three dimensional random fibre networks, *i.e*. those with fibre centres distributed according to a point Poisson process in three dimensions and with uniform orientation of fibre axes within the solid angle 2π.

Inter-fibre contacts

Corte and Kallmes [73] refer to the result of Miles who, for a three dimensional random fibre network, gives the total number of fibre crossings, $n_{cross,v}$ made by n_v fibres in a volume V as

$$n_{cross,v} = \frac{\pi}{2} n_v^2 \frac{\bar{\lambda}^2 r_f}{V} \qquad \text{for } V \gg \bar{\lambda}^3 \tag{29}$$

where r_f is the fibre radius (m). An expression equivalent to Equation (29) was obtained some years later by Komori and Makishima [74].

Typically of more interest is the mean number of contacts per fibre, $\bar{n}_{con} = 2\, n_{cross,v} / n_v$ where the factor 2 is introduced since each crossing produces a contact point on each fibre. Observing that for cylindrical fibres, the volumetric fibre consistency C_v is given by

$$C_v = \frac{n_v \pi \bar{\lambda} r_f^2}{V} \tag{30}$$

we have

$$\bar{n}_{con} = \pi n_v \frac{\bar{\lambda}^2 r_f}{V} \tag{31}$$

$$= \frac{\bar{\lambda}}{r_f} \left(\frac{n_v \pi \bar{\lambda} r_f^2}{V} \right) \tag{32}$$

$$= 2\, A C_v . \tag{33}$$

By definition, and from Equation (4)

$$C_m = \frac{n_v \bar{\lambda} \delta}{V} \tag{34}$$

$$= \frac{6\,\delta}{\pi \bar{\lambda}^2} n_{crowd} \tag{35}$$

we have therefore

$$\bar{n}_{con} = \pi \left(\frac{n_v \bar{\lambda}}{V} \right) \lambda r_f \tag{36}$$

$$= \pi \frac{C_m}{\delta} \bar{\lambda} r_f \tag{37}$$

$$= \frac{3}{A} n_{crowd} \tag{38}$$

More recently, Equations (33) and (38) were derived fully and independently by Dodson [75] following the methods of van Wyk [76]; Equation (33) is given also without derivation by Toll [77].

Meyer and Wahren [78] relate the volumetric concentration to the number of contacts per fibre by the expression

$$C_v = \frac{16\pi A}{\left(\frac{2A}{\bar{n}_{con}} + \frac{\bar{n}_{con}}{\bar{n}_{con} - 1}\right)^3 (\bar{n}_{con} - 1)} \tag{39}$$

Modified theories of fibre contact, which seek to account for the reduction in length due to existing contacts, have been derived by, *e.g.* Pan [79] who gives,

$$\bar{n}_{con} = \frac{4AC_v}{2 + \pi C_v} \tag{40}$$

The approach taken by Pan has been criticized by Komori and Itoh [80] who present a modification of their own which has an iterative solution for all cases other than when $\bar{n}_{con} \to \infty$; the differences in approach are summarized by Pan [81]. It should be noted however that where true three dimensional fibre networks exist in papermaking operations, we typically have low C_v and n_{con}; accordingly these corrections have little influence. Equations (33), (39) and (40) are compared in Figure 8 for a typical headbox consistency, $C_v = 3\,\%$ and a typical thick-stock consistency $C_v = 10\,\%$. We note that, as expected from the modification, Equation (40) gives a lower estimate of $\bar{n}_{con}$ than that given by Equation (33); Equation (39) however may under- or over-estimate the mean number of contacts depending on the value of C_v and the aspect ratio.

The mean number of contacts per fibre is not only relevant to the strength and rheology of a fibre suspension, it defines also the threshold at which we expect flocs to form by elastic fibre bending. For contacts on a given fibre

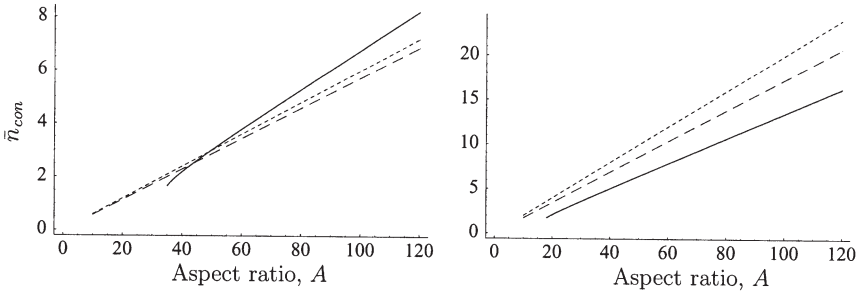

Figure 8 Mean number of contacts per fibre plotted against fibre aspect ratio. Left: $C_v = 3\,\%$; right: $C_v = 10\,\%$. Key: solid line – Equation (39); dotted line – Equation (33); broken line – Equation (40).

Table 1 Critical crowding number required for flocs formed by elastic fibre bending.

$\bar{n}_{con}$	n_{crowd} calculated by		
	Kerekes	Equation (38)	Equation (40)
3	60	A	$\frac{4A^2}{4A-3\pi}$
4	90	$\frac{4}{3}A$	$\frac{4A^2}{3(A-\pi)}$

occurring on alternate sides of the fibre axis this threshold is $n_{con} = 3$ though more typically we might expect $\bar{n}_{con} = 4$. Kerekes and Schell [8] used a simplification of Equation (39) to estimate the crowding number where these values of $\bar{n}_{con}$ occur; their estimates along with those determined using Equations (38) and (40) are given in Table 1. It should be noted that the value of $n_{crowd} = A$ at $\bar{n}_{con} = 3$ was given by Dodson in [75] who related this to the concentration where coherent networks form from the sedimentation of dilute fibre suspensions. The difference between the estimates of these critical values of n_{crowd} obtained via Equations (38) and (40) is less than 5 % for $A > 50$; the primary importance of determining this critical crowding number in this way is that it is defined by fibre geometry.

Naturally, the strength properties of a fibre suspension will be affected not only by the number of contacts but by the area of these contacts. In a simulation study, Wang and Shaler [82] found that the contact area was distributed according to a modified lognormal distribution.

The maximum volumetric consistency obtained by the random placement of rods in a three dimensional assembly until no more rods may be fitted is given by Parkhouse and Kelly [83] as

$$C_v^{max} = 2\frac{\log(A)}{A} \tag{41}$$

which, using Equation (33), corresponds to $\bar{n}_{con} = 4\log(A)$.

Evans and Gibson [84] modelled the maximum volumetric consistency as that when each rod is restricted from rotational motion by its neighbours and give the expression

$$C_v^{max} = \frac{4}{A} \tag{42}$$

which, using Equation (33), corresponds to $\bar{n}_{con} = 8$.

Recently, Novellani *et al*. [85] presented measurements of the mean porosity in 3D networks and found good agreement with the theory of Rahli who gave:

$$C_v^{max} \approx \frac{11}{\frac{\pi}{2A} + 2A + 6} \tag{43}$$

where the numerator is determined by the equivalent number of fibres in an excluded volume defined as the mean fractional volume which a given fibre prevents the centre of surrounding fibres from occupying and is found to be constant and approximately equal to 11 for $A > 7$.

Porosity distribution

The porosity distribution in a three dimensional network is, by definition, the complement of the local consistency distribution. Knowledge of the porosity distribution therefore provides a reference statistic against which the nonuniformity of flocculated suspensions may be compared. Analytic approaches to this property of network structure are few though Dodson and Sampson [86] recently derived the variance of local consistency by expressing Equation (33) in terms of the local properties of the network such that

$$\tilde{n}_{con} = 2A(1 - \tilde{C}_v) \tag{44}$$

$$\sigma_x^2(\tilde{C}_v) = \frac{\sigma_x^2(\tilde{n}_{con})}{4A^2} \tag{45}$$

where $\sigma_x^2(\tilde{C}_v)$ and $\sigma_x^2(\tilde{n}_{con})$ represent the variances of the local average volumetric consistency and the local average number of contacts per fibre for cubic inspection volumes of side x respectively.

If fibre contacts are given by a Poisson process then, by the Central Limit Theorem, the variance of fibre contacts, $\sigma_x^2(\tilde{n}_{con})$ is given by the mean number of fibre contacts divided by the mean number of fibres in a given volume. On manipulation this yields, for cylindrical fibres,

$$\sigma_x^2(\tilde{C}_v) = \frac{\pi}{8}\left(\frac{\omega}{x}\right)^3 \tag{46}$$

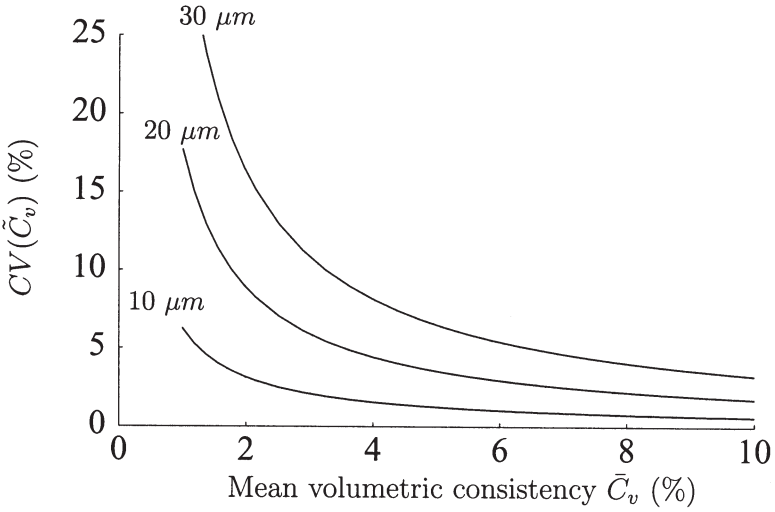

Figure 9 Coefficient of variation of volumetric consistency plotted against mean volumetric consistency for random 3D networks. Curves shown for fibre width, $\omega = 10, 20, 30\ \mu m$; inspection volume size 1 mm^3.

where ω is the fibre width (m). The result is striking; at a given inspection volume size, the variance of local consistency in a random three dimensional network is dependent only on the cube of the fibre width and is independent of the mean volumetric consistency. The coefficient of variation of local consistency, calculated using Equation (46) is plotted against the mean local consistency in Figure 9 for $x = 1\ mm$.

The pore radius distribution in 3D networks is difficult to define, though the recent algorithms of Luchnikov *et al*. [87] show some potential for such studies. Luchnikov *et al*. have developed algorithms allowing Voronoi networks, which characterise the void space of a system, to be used for the study of non-spherical objects and present preliminary analysis of a 3D system of random lines. Some progress on the analytic description of void space in 3D networks has been made recently by Philipse and Kluijtmans [88] who considered the caging of spheres by random networks of rods.

MODELLING PLANAR NETWORKS

Typically the thickness of a sheet of paper is of order one tenth or less of a mean fibre length and thus, as we have seen in the discussion of experimental techniques to characterise sheet structure, several features of importance may be quantified through measurements made of projections of the structure onto a plane. Note also that Radvan, Dodson and Skold showed that, as a consequence of the dynamics of the sheet forming process, the *z*-directional structure of the sheet is predominantly layered rather than felted [89], *i.e.* along their length, fibres lie predominantly in the plane of the sheet. Accordingly, when modelling the structure of such 'near-planar' networks, many workers have considered the statistical geometry of idealised two-dimensional networks and it is these models that are considered here.

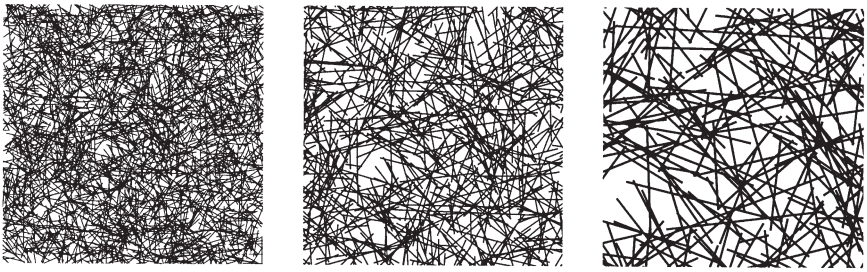

Figure 10 Random network of fibres with mean length 1 *mm*, mean width 20 μm, coarseness 2×10^{-4} $g\ m^{-1}$, mean network grammage 5 $g\ m^{-2}$, mean coverage 0.5; fibre lengths lognormally distributed with coefficient of variation 50 %. Left: 1 $cm \times 1$ *cm*; centre: 0.5 $cm \times 0.5$ *cm*; right: 0.25 $cm \times 0.25$ *cm*; centre point of each image is the same.

Random networks

The first attempt to model paper structure using statistical geometry was given by Kallmes and Corte [90], a revised, expanded and perhaps more accessible treatise is given in the proceedings of these symposia [73]. They derived expressions for several structural features of random fibre networks which are considered in the following sections. Importantly, Corte and Kallmes gave precisely the definition of a two-dimensional random fibre network:

- The fibres are deposited independently of one another.
- The fibres have an equal probability of landing at all points in the sheet, *i.e.* the fibre centres are randomly distributed over the area.
- The fibres have an equal probability of making all possible angles with any arbitrarily chosen, fixed axis, *i.e.* the fibres have a random orientation.

So in modelling the structure of two-dimensional random fibre networks we consider fibres centres to be distributed according to a point Poisson process in two dimensions and fibre axes to have a uniform distribution within an angle π relative to some arbitrary direction. Illustrative examples of such random networks are given in Figure 10.

Mass distribution

As has been discussed, the statistics used to characterise the mass distribution in a sheet, as measured by, for example β-radiography and image analysis, are derived from the observed variance of local grammage at a given scale of inspection. The variance obtained in a random fibre network, as defined above, was derived by Dodson [91, 92] and discussed in detail in [12]. Here, the key stages of the derivation only are given, along with the applicable results with have seen substantial use by workers in the paper science literature.

Modelling fibres as uniform rectangles of length λ, width ω, where $\lambda > \omega$ and coarseness δ we have fibre grammage, $\beta_{fib} = \delta/\omega$ and fibre area, $a_{fib} = \lambda\omega$. So, in a sheet of mean grammage $\bar{\beta}$, the average number of fibres covering a *point* is given by

$$\bar{c} = \frac{\bar{\beta}}{\beta_{fib}} \tag{47}$$

and, since for Poisson processes the variance is equal to the mean, we have

$$\sigma^2(c) = \bar{c} \tag{48}$$

$$= \frac{\bar{\beta}}{\beta_{fib}} \tag{49}$$

$$= \frac{\omega}{\delta}\bar{\beta} \tag{50}$$

Whilst it is perhaps a little counter-intuitive to consider the point variance of

grammage, it follows directly from Equation (50) that this parameter is given by

$$\sigma^2(\beta) = \frac{\delta}{\omega}\bar{\beta} \tag{51}$$

In any real sampling scheme for fibre networks, we must make observations and measurements on finite areas instead of points. Kallmes and Corte [90] point out that when considering the number of fibres in a square zone of side x, as opposed to the number covering a point, all fibres longer than $\sqrt{2}x$, and most of those longer than $x/2$ will have a portion of their length, and hence mass, in squares adjacent to any given square. In their determination of the distribution of the total fibre length per unit area, Kallmes and Corte overcame this problem by considering a point Poisson process for fibre *segments*. For determination of the distribution of local grammage in two-dimensional random networks, Dodson [91, 92] derived instead the *fractional between zones variance* $\tilde{\rho}$, which weights the point variance to yield the variance observed at finite scales of inspection. We shall consider only square inspection zones of side x such that

$$\sigma_x^2(\tilde{\beta}) = \sigma^2(\beta)\tilde{\rho} \tag{52}$$

$$= \frac{\delta}{\omega}\bar{\beta}\tilde{\rho} \tag{53}$$

and

$$CV_x(\tilde{\beta}) = \sqrt{\frac{\delta}{\omega}\frac{\tilde{\rho}}{\bar{\beta}}} \tag{54}$$

Parameter $\tilde{\rho}$ is given by

$$\tilde{\rho} = \int_0^{\sqrt{2}x} a(r,\omega,\lambda)\, b(r,x)\, dr \tag{55}$$

where $a(r,\omega,\lambda)$ is the *point autocorrelation function* for coverage at points separated by a distance r and $b(r, x)$ is the probability density function for the distance r between two points chosen independently and at random within

the inspection zone. For square zones of side x, these functions are given by Dodson [92] as:

$$a(r,\omega,\lambda) = \begin{cases} 1 - \frac{2}{\pi}\left(\frac{r}{\lambda} + \frac{r}{\omega} - \frac{r^2}{2\omega\lambda}\right) & \text{for } 0 < r \le \omega \\ \frac{2}{\pi}\left(\arcsin\left(\frac{\omega}{r}\right) - \frac{\omega}{2\lambda} - \frac{r}{\omega} + \sqrt{\frac{r^2}{\omega^2} - 1}\right) & \text{for } \omega < r \le \lambda \\ \frac{2}{\pi}\left(\arcsin\left(\frac{\omega}{r}\right) - \arccos\left(\frac{\lambda}{r}\right) - \frac{\omega}{2\lambda} - \frac{\lambda}{2\omega}\right. & \\ \qquad \left. - \frac{r^2}{2\lambda\omega} + \sqrt{\frac{r^2}{\lambda^2} - 1} + \sqrt{\frac{r^2}{\omega^2} - 1}\right) & \text{for } \lambda < r \le \sqrt{\lambda^2 + \omega^2} \\ 0 & \text{for } r > \sqrt{\lambda^2 + \omega^2} \end{cases} \tag{56}$$

and

$$b(r,x) = \begin{cases} \frac{4r}{x^4}\left(\frac{\pi x^2}{2} - 2rx + \frac{r^2}{2}\right) & \text{for } 0 \le r \le x \\ \frac{4r}{x^4}\left(x^2\left(\arcsin\left(\frac{x}{r}\right) - \arccos\left(\frac{x}{r}\right)\right)\right. & \\ \left. + 2x\sqrt{r^2 - x^2} - \frac{1}{2}(r^2 + 2x^2)\right). & \text{for } x \le r \le \sqrt{2}x \\ 0 & \text{for } r > \sqrt{2}x \end{cases} \tag{57}$$

respectively and Equations (57) are attributable to Ghosh. Numerical integration of Equations (56) and (57) for known values of fibre length and width allows calculation of the fractional between zones variance $\tilde{\rho}$ for square zones of side x; note that the same length dimension, *e.g. mm* should be used for each variable. Where there is a distribution of lengths, $\tilde{\rho}_i$ should be determined for each fibre length class λ_i and, since the variance contributions of each length fraction are additive, the total fractional between zones variance is given by

$$\tilde{\rho} = \sum_{i}^{n} m_i \tilde{\rho}_i \,, \tag{58}$$

where m_i is the mass fraction of fibres with class centre λ_i. The treatment assumes uniform fibre width. Tables of $\tilde{\rho}_i$ calculated for square zones of side 1, 2, 3 and 4 *mm* for fibre lengths in increments of 0.2 *mm* and a fibre width of

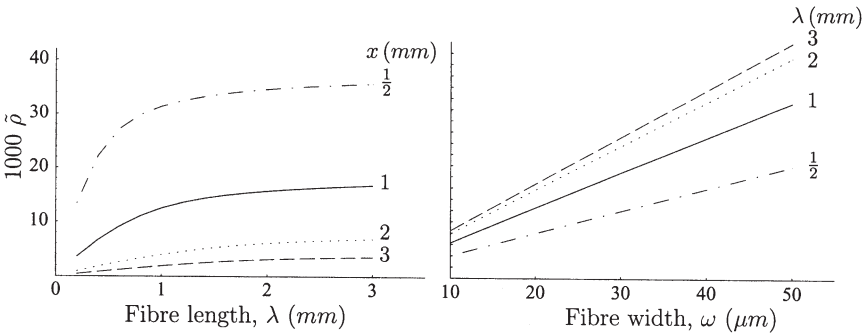

Figure 11 Effect of fibre length, fibre width and inspection zone size on the fractional between zones variance, $\tilde{p}$. Left: effect of fibre length and inspection zone size when $\omega = 20\ \mu m$; right: effect of fibre width and length when $x = 1\ mm$.

20 μm can be found in [93] and in the appendix to [12]. Where there is a distribution of fibre lengths, the coefficient of variation of local grammage is reduced by a few percent when compared to that of fibres of uniform length and the same mean [11].

The fractional between zones variance $\tilde{p}$ for square inspection zones of side x is plotted against fibre length and fibre width in Figure 11; we observe that it increases monotonically with decreasing gradient with fibre length and is proportional to fibre width over the range of interest for papermaking fibres, *i.e.* where fibre width is small compared to both length and inspection zone size [94]. Note also, whilst not plotted here, that $\tilde{p}$ decreases monotonically with decreasing gradient for increasing inspection zone size, x.

Now, for small zones, $\tilde{p} \to 1$ and the variance of local grammage $\sigma_x^2(\tilde{\beta})$ approaches the point variance given by Equation (51) [38]. For large zones, $x \gg \lambda$ and the mean number of fibres in a zone of side x is[1]

$$\bar{n}_x = \frac{\bar{c}x^2}{\lambda\omega} \tag{59}$$

and, since we have a Poisson process, the variance $\sigma_x^2(\tilde{n}_x)$ is the same. A large zone containing $\tilde{n}_x$ fibres has grammage

$$\tilde{\beta} = \frac{\lambda\delta}{x^2}\ \tilde{n}_x \tag{60}$$

[1]Equation (59) corrects the typographical errors on Page 103 of [12].

and hence the variance of local grammage is

$$\sigma_x^2(\tilde{\beta}) = \sigma_x^2\left(\frac{\lambda\delta}{x^2}\,\tilde{n}_x\right) \tag{61}$$

$$= \left(\frac{\lambda\delta}{x^2}\right)^2 \bar{n}_x \tag{62}$$

after substituting for $\bar{n}_x$ from Equation (59) and observing that $\bar{\beta} = \delta\ \bar{c}/w$, rearranging Equation (62) yields

$$\sigma_x^2(\tilde{\beta}) = \frac{\lambda\delta}{x^2}\,\bar{\beta}. \tag{63}$$

Corte and Dodson [38] modified Equation (63) to take account of autocorrelation such that

$$\sigma_x^2(\tilde{\beta}) = \frac{\lambda\delta}{x^2}\,\bar{\beta}\,\aleph. \tag{64}$$

where $0 \le \aleph \le 1$ and is a function of fibre geometry and the inspection zone size. Comparison of Equation (64) with Equation (53) yields

$$\aleph = \frac{x^2}{\lambda}\,\frac{\tilde{\rho}}{\omega}. \tag{65}$$

We observe that $\aleph$ is therefore a weighted form of the fractional between zones variance $\tilde{\rho}$; the weighting being given by the ratio of the area of an inspection zone to that of a rectangular fibre.

Corte and Dodson [38] derived expressions for $\aleph$ using a technique referred to as the 'line method'. The analysis involved trigonometric determination of the overlapping distance of random lines of length λ and angle ϑ with centres occurring within square zones of side x. Three different functions determine $\aleph$, each applying to a given range of λ as a multiple of x. Errors in the equations given in the original article [38] were apparently corrected in a subsequent publication [95]; since then they have appeared in several publications, *e.g.* pp207–208 in [94], [96, 97] and widely circulated translations of [38]. The second part of these equations is incorrect in every publication seen by this author; the full derivation was not given in [38] but brief instructions to

determine the integrals were. These have been recalculated and the resulting expressions for $\varkappa$ are given as follows:

$$\varkappa = \begin{cases} 1 - \dfrac{4}{3\pi}\dfrac{\lambda}{x} + \dfrac{1}{6\pi}\dfrac{\lambda^2}{x^2} & \text{for } \lambda \le x \\ \dfrac{4}{\pi}\left(\dfrac{x}{\lambda}\left(\log\left(\dfrac{x}{\lambda}\right) - \log\left(1 - \sqrt{1 - \dfrac{x^2}{\lambda^2}}\right)\right) + \arcsin\left(\dfrac{x}{\lambda}\right)\right. & \\ \qquad \left. + \dfrac{(\lambda^2 - x^2)^{\frac{3}{2}}}{3x\lambda^2}\right) - \dfrac{1}{6\pi}\dfrac{\lambda^2}{x^2} + \dfrac{4}{3\pi}\dfrac{x}{\lambda} - \dfrac{1}{3\pi}\dfrac{x^2}{\lambda^2} - \dfrac{2}{\pi} - 1 & \text{for } x \le \lambda \le \sqrt{2}x \\ \dfrac{1}{\pi}\left(4\dfrac{x}{\lambda}\left(\dfrac{1}{3}(1 - \sqrt{2}) + \log(1 + \sqrt{2})\right) - \dfrac{x^2}{\lambda^2}\right) & \text{for } \lambda \ge x\sqrt{2} \end{cases} \tag{66}$$

There is no doubt that Equations (66) were derived correctly by Corte and Dodson [38] since they have been plotted correctly as a function of λ and x at least twice [94, 97]. The function is plotted in Figure 12 against λ/x. For completeness, Equations (66) are given with coefficients in decimal form in Appendix 1 along with a table of $\varkappa$ over the range of interest of λ/x.

The line method is compared with the analytic formula in Figure 13 for fibres of width 30 μm. Agreement between the two methods is excellent; the greatest error occurs for small x and λ and is less than 0.25 % for the data plotted. Note that the line method makes implicit use of the observed proportionality between $\tilde{\rho}$ and ω illustrated in Figure 11. Where there is a distribution of lengths, a similar treatment should be used for $\varkappa$ as that used for $\tilde{\rho}$ such that

$$\begin{aligned} \sigma_x^2(\tilde{\beta}) &= \frac{\delta}{x^2}\bar{\beta}\lambda\varkappa, \\ &= \frac{\delta}{x^2}\bar{\beta}\sum_i^n m_i\lambda_i\varkappa_i, \end{aligned} \tag{67}$$

The coefficient of variation of local grammage at the 1 *mm* scale of inspection, calculated using the line method, is plotted in Figure 14 for the typical ranges of coarseness and fibre length found in papermaking systems. The mean grammage for the curves plotted in Figure 14 is 60 $g\,m^{-2}$. An advantage of the line method over the determination of the fractional between zones variance is that parameter $\varkappa$, and hence the variance and coefficient of variation of local grammage, may be determined without knowledge of fibre width. Thus, knowing fibre coarseness and length, the coefficient of variation

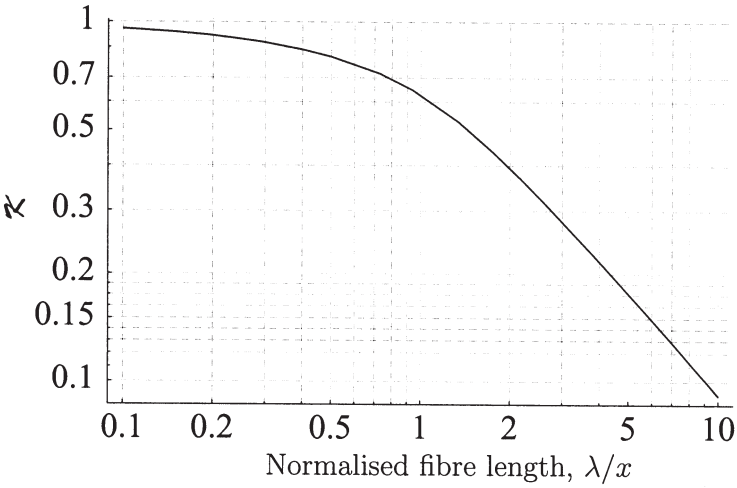

Figure 12 Parameter $\varkappa$ as a function of fibre length and inspection zone size.

of local grammage at the 1 *mm* scale may be read off the scales of Figure 14; for networks of mean grammage other than 60 $g\,m^{-2}$, the value read from the ordinate should be multiplied by $\sqrt{60/\bar{\beta}} \approx 7.75/\sqrt{\bar{\beta}}$. Note also that there is some evidence that fibre coarseness is, at least to a first approximation, proportional to fibre length [98]; so for a range of fibre lengths and coarsenesses, we might expect a plot of $CV\,(\tilde{\beta})$ against $\sqrt{\lambda\bar{\delta}}$ to be approximately linear and to fall within the envelope shown in Figure 14.

The wavelength power spectrum for random fibre networks was derived by Haglund *et al*. [99]. It may be computed as the Fourier transform of the point autocorrelation function $a(r,\omega,\lambda)$ [12], but is most widely applied in the form given by Haglund *et al*. [99]:

$$\mathcal{P}\left(\frac{l}{\omega}\right) = \frac{1}{\bar{c}}\frac{16}{\pi^2}\frac{\lambda}{\omega}\left(\frac{\omega}{l}\right)^2 \int_{\frac{\pi\omega}{l}}^{\infty} \left(\left(\frac{J_1(y\phi/\omega)}{y\phi/\omega}\right)^2 \left(1-\left(\frac{\pi\omega}{yl}\right)^2\right)^{-\frac{1}{2}} \times \int_{-\frac{\pi}{2}}^{\frac{\pi}{2}} \frac{\sin^2(y\lambda\cos(t)/\omega)}{(y\lambda\cos(t)/\omega)^2}\frac{\sin^2(y\sin(t))}{(y\sin(t))^2}.dt\right).dy \qquad (68)$$

where ϕ is the diameter of a circular scanning aperture (*mm*) and $J_1(\zeta)$ is the first order Bessel function. Since the power spectrum for random fibre networks, as given by Equation (68) is inversely proportional to the mean

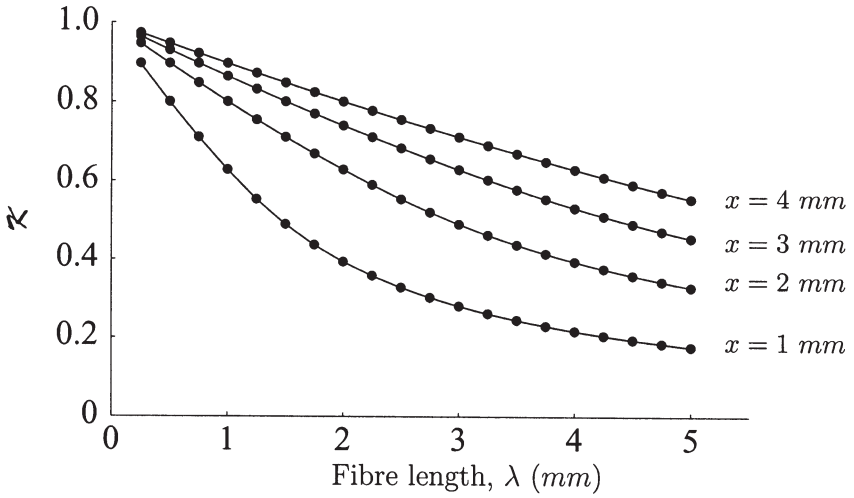

Figure 13 Comparison of $\varkappa$ determined by Equations (65) and (66). Points calculated using Equations (66), lines calculated using Equations (65); all curves calculated for $\omega = 30\ \mu m$. Agreement between the two methods is excellent.

coverage $\bar{c}$, changes in mean basis weight cause a vertical shift in the spectrum. Integrating Equation (68) from ϕ to infinity yields the coefficient of variation of local coverage denoted the *total formation* by Haglund *et al*. [99]; when $\phi = 0$ the integrals recover the Poisson result,

$$CV(c) = \frac{1}{\sqrt{\bar{c}}}. \tag{69}$$

Peculiarly, and without justification, Norman states that consideration of a point Poisson process to arrive at Equation (69) is a rather heuristic process [100]. As we have seen for the fractional between zones variance, and parameter $\varkappa$ determined via the line method, where there is a distribution of geometries, variances are additive so Equation (68) is evaluated for each fibre length or width of interest with the appropriate value of $\bar{c}$ for that component in the furnish, and the spectra summed.

The power spectrum for random networks is plotted for fibres of differing aspect ratio and $\phi = 0$ in Figure 15; spectra have been computed for unit mean coverage. The spectra are similar at low wavelengths though at higher wavelengths, the spectral density is greater at higher aspect ratios. The influence of

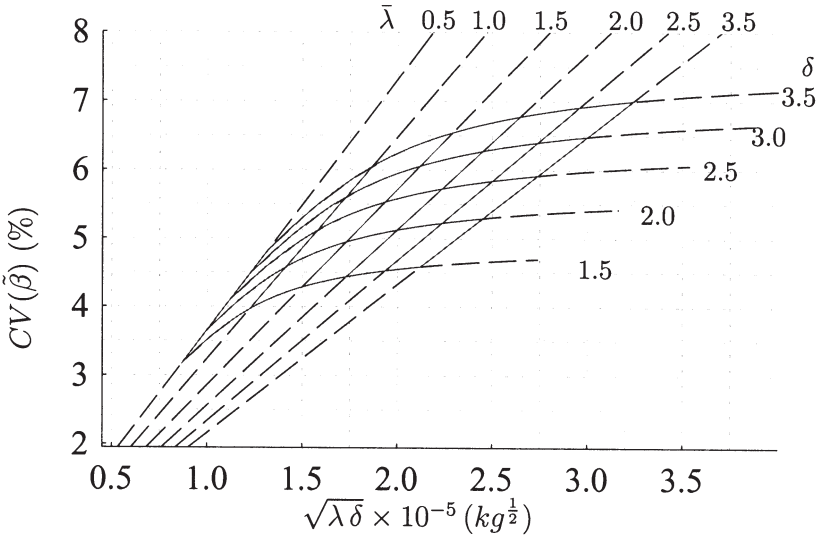

Figure 14 Coefficient of variation of local grammage at 1 *mm* scale for random networks of mean grammage 60 $g\ m^{-2}$ as a function of mean fibre length and coarseness. Units of coarseness δ are $10^{-4} g\ m^{-1}$; units of mean fibre length $\bar{\lambda}$ are *mm*.

finite ϕ is to reduce the density and to shift the spectra to the right; the reduction in density being greater for low aspect ratios and the maximum of the spectra occurs at a wavelength around 2 ϕ [99].

Through combination of Equations (25) and (68), Jordan and Nguyen [51] determined also the specific perimeter for random fibre networks.

The importance of modelling random fibre networks is not, as we shall see, that they describe the structure of commercially formed sheets which depart from randomness because of, *e.g.* fibre flocculation and fibre orientation. Their role is as reference structures against which the measured properties of real sheets may be compared.

Comparative quantifiers of mass distribution

Comparison of measurements of the mass distribution made on real sheets using, for example, β-radiography and image analysis, with those calculated for random fibre networks with the same furnish morphologies allows insights into the mechanisms of forming. Here, quantitative descriptors of the difference between real and random networks are presented.

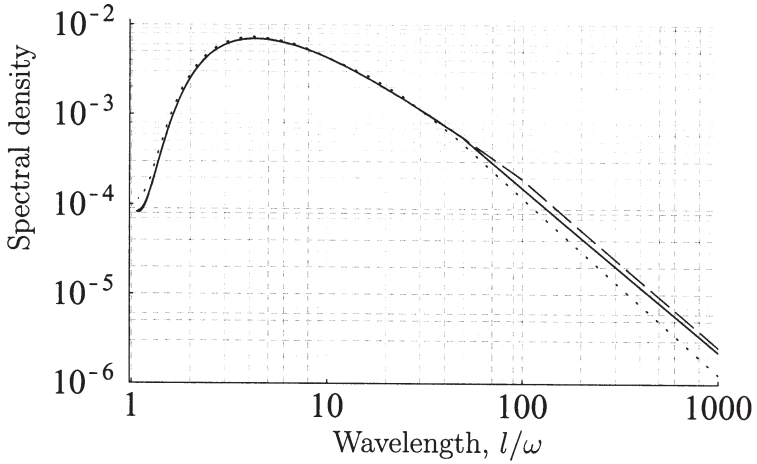

Figure 15 Power spectra for random networks. Plots are given for measuring area $\phi = 0$ and mean coverage $\bar{c} = 1$. Dotted line: Aspect ratio $A = 10$; solid line: $A = 50$; dashed line $A = 100$.

Perhaps the earliest statistic proposed to measure the deviation of the mass distribution of real papers from that calculated for random networks is the nonuniformity number U_x proposed by Corte and Dodson [38] and defined by

$$U_x = \frac{\sigma_x^2(\tilde{\beta})_{meas} - \sigma_x^2(\tilde{\beta})_{rand}}{\sigma_x^2(\tilde{\beta})_{meas} + \sigma_x^2(\tilde{\beta})_{rand}}, \tag{70}$$

where the subscripts *meas* and *rand* denote measured and random variances respectively. For a paper with a greater variance than a random network formed from the same fibres at a given scale of inspection x, $\sigma_x^2(\tilde{\beta})_{meas} > \sigma_x^2(\tilde{\beta})_{rand}$ and hence $0 < U_x \leq 1$; similarly, a sheet with smaller variance than a random network formed from the same fibres, $\sigma_x^2(\tilde{\beta})_{rand} > \sigma_x^2(\tilde{\beta})_{meas}$ and $-1 \leq U_x < 0$. A network with the same variance observed for a random network will have $U = 0$.

Corte [95, 97] subsequently proposed quantifying the departure of real papers from randomness using the *variance ratio*. This measure has since been used extensively by Dodson and co-workers, *e.g.* [12] and has been termed the *formation number*, $n_{f,x}$; it is defined as

$$n_{f,x} = \frac{\sigma_x^2(\tilde{\beta})_{meas}}{\sigma_x^2(\tilde{\beta})_{rand}}. \tag{71}$$

When $\sigma_x^2(\tilde{\beta})_{meas} > \sigma_x^2(\tilde{\beta})_{rand}$ the formation number $n_{f,x} > 1$, and when $\sigma_x^2(\tilde{\beta})_{rand} > \sigma_x^2(\tilde{\beta})_{meas}$ we have $n_{f,x} < 1$. A network with the same variance observed for a random network will have $n_{f,x} = 1$.

The terms 'formation number' and *formation intensity* have been applied also by Norman and Wahren and co-workers, *e.g.* [15, 100, 101], to the coefficient of variation of local grammage, *i.e.* without comparison with random networks. Here, the term 'formation number' will be applied to the statistic given by Equation (71) and the coefficient of variation of local grammage will be referred to as such; the choice is arbitrary and it is unfortunate that conflicting definitions exist. It is important however that workers specify precisely which definition is used in a given study.

An approximation of $n_{f,x}$ was proposed by Schaffnit [102] and its use is discussed by Ng and Dodson [103]. It is arrived at by replacing the variance of a random network in Equation (71) with that measured from a laboratory handsheet formed from the same furnish as the paper under investigation $\sigma_x^2(\tilde{\beta})_{hls}$, such that

$$n_{f,x}^{est} = \frac{\sigma_x^2(\tilde{\beta})_{meas}}{\sigma_x^2(\tilde{\beta})_{hls}}, \tag{72}$$

The technique relies on the low crowding number, n_{crowd} in the chamber of the sheet former which allows little interaction between fibres such that the formed sheet has similar mass distribution to a random network and $n_{f,x} \approx 1$. Schaffnit reports that $n_{f,x}^{est}$ overestimates $n_{f,x}$ by about 5 % at the 1 *mm* scale.

Comparison of the power spectrum for a sample with that obtained for a random network is typically achieved by plotting spectra on the same axes and observing differences in the height of the spectrum [99]. Quantitative analysis may be carried out by integrating the spectra between given wavelengths and comparing the values of the integrals, or by determination of the micro- and macro-scale characteristic lengths, as described earlier and given by Equations (17) and (18) respectively.

Number of crossings per fibre

The number of contacts per fibre necessarily controls the mean distance between crossings for fibres of given length and width. These properties of random networks were studied by Kallmes and Corte [90] who made

comparative measurements on real fibre networks. Following Kallmes and Corte we shall consider first '2-D' networks, *i.e.* networks where, " . . . the number of fibres in the network is so small that the area covered by more than two fibres is negligible, *i.e.* less than 1 % . . . " [90]; consideration of the Poisson distribution shows that this criterion is satisfied for networks with mean coverage $\bar{c} \leq 0.456$, which, for typical fibres corresponds to a mean grammage $\bar{\beta}$ up to about 2 $g\ m^{-2}$. Naturally such networks are not necessarily representative of real papers which have a significant structural component in the third dimension; accordingly the treatments for 2-D networks are developed for application to multi-layer structures.

For 2-D networks Kallmes and Corte note that the number of intersections between $\bar{n}_x$ fibres within an area x^2 is given by the product of the probability that two fibres intersect and the number of ways that pairs of fibres may be selected [90]. The probability that two *lines* intersect at angle ϑ is given by $\lambda^2/x^2 \sin(\vartheta)$, so for all ϑ the probability of intersection is

$$P_{cross} = \frac{2}{\pi}\frac{\lambda^2}{x^2}\int_0^{\frac{\pi}{2}} |\sin(\vartheta)|.d\vartheta = \frac{2}{\pi}\frac{\lambda^2}{x^2} \tag{73}$$

and each fibre can intersect all fibres except itself, so for $\bar{n}_x$ fibres, the number of ways that pairs of fibres may be selected is $n_x(n_x - 1)/2$ where the divisor 2 is applied because each fibre is counted twice. Thus, the expected number of crossings *per unit area* is given by

$$\bar{n}_{cross} = \frac{1}{\pi}\frac{\lambda^2}{x^4}\bar{n}_x(\bar{n}_x - 1) \tag{74}$$

$$\approx \frac{\lambda^2 \bar{n}_x^2}{\pi x^4} \qquad \text{for } \bar{n}_x \gg 1 \tag{75}$$

substituting for $\bar{n}_x$ from Equation (59)

$$\bar{n}_{cross} \approx \frac{\bar{c}^2}{\pi\omega^2} \tag{76}$$

Also of importance is the expected number of crossings *per fibre*, which is given by Kallmes and Corte as

$$\bar{n}_{cross,\,fib} = 2\frac{\bar{n}_{cross}x^2}{\bar{n}_x} \tag{77}$$

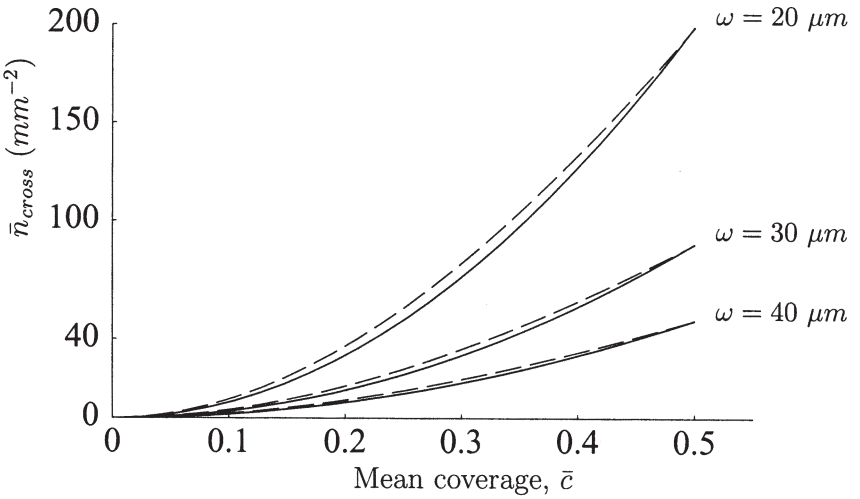

Figure 16 Number of contacts per square millimetre $\bar{n}_{cross}$ for 2-D networks plotted against mean coverage. Solid lines, Equation (76); dashed lines, Equation (80).

and thus we have

$$\bar{n}_{cross,\,fib} = \frac{2}{\pi}\frac{\lambda^2}{x^2}(\bar{n}_x - 1) \tag{78}$$

$$\approx \frac{2}{\pi}\frac{\bar{c}\lambda}{\omega} = \frac{2\bar{c}A}{\pi} \qquad \text{for } \bar{n}_x \gg 1 \tag{79}$$

Dodson [12] considered the fraction of a 2-D network with coverage of two and three fibres according to the Poisson distribution and the area of a fibre crossing, $\omega^2/\sin(\vartheta)$ to arrive at

$$\bar{n}_{cross} = \frac{\pi}{4}\frac{\bar{c}^2}{\omega^2}\left(\frac{1}{2} + \frac{\bar{c}}{3}\right)e^{-\bar{c}} \tag{80}$$

As illustrated in Figure 16, over the applicable range of fibre widths and coverage, Equation (80) yields a slightly higher estimate of $\bar{n}_{cross}$ than Equation (76) since fibre width and regions with coverage up to three are included.

Kallmes, Corte and Bernier [104] developed the single layer concept given in [90] for multi-layer, or *multi-planar* (MP), structures. They considered the number of crossings *within* a given layer, as given above, and the number of crossings *between* fibres in pairs of layers, noting that the top and bottom layers have between-layer contacts with respectively the layers below and above them only. For a multi-planar sheet with n_l layers, the expected number of crossings per unit area is given by

$$\bar{n}_{cross}^{MP} = \bar{n}_{cross}\frac{n_l}{2}(1+e^{-\bar{c}})\left(f_w + (1+e^{-\bar{c}})\left(\left(1-\frac{1}{n_l}\right)\left(f_b + \frac{C\,e^{-2\bar{c}}}{1-e^{-2\bar{c}}}\right) - \frac{C\,e^{-2\bar{c}}(1-e^{-2(n_l-1)\bar{c}})}{n_l(1-e^{-2\bar{c}})^2}\right)\right), \quad (81)$$

where f_w and f_b are the effective fibre flexibilities within and between adjacent layers respectively and C is approximately constant and given by $C = f_f\, e^{\bar{c}}$ where f_f is the effective fibre flexibility of fibres generating crossings between layers separated by a layer. Experimentally determined values of effective fibre flexibilities were given by Kallmes *et al*. [104] for unbeaten, unbleached kraft and sulphite spruce pulps and these are given in Table 2.

Table 2 Effective fibre flexibilities for multi-planar sheets as given in [104].

Pulp	Pressing *psi*	f_w	f_b	f_f
Sulphite	1000	0.95	0.89	0.64
	50	0.92	0.71	0.44
Kraft	1000	0.84	0.65	0.37
	50	0.74	0.51	0.27

The number of crossings per fibre in a multi-planar sheet is given by

$$\bar{n}_{cross,\,fib}^{MP} = 2\,\frac{\bar{n}_{cross}^{MP} x^2}{\bar{n}_x n_l}. \quad (82)$$

The number of crossings per fibre is plotted in Figure 17 using data given in Table 2 for the sulphite pulp pressed at 6.9 *MPa* (1000 *psi*) with an aspect ratio of 60; mean coverage of a layer was assumed to be 0.4. The broken line in Figure 17 represents the same data with the flexibility $f_f = 0$ such that fibre

contacts are assumed to occur only between adjacent layers; the important feature of this curve is that it reaches an asymptote for n_l greater than about 5. This agrees with expectation since the outer layers are in contact with other layers on one side only, and the number of contacts per fibre will be insensitive to the contribution of outer layers for fibres located more than two layers from the surface. We can estimate this number of contacts per fibre taking the limit of $\bar{n}^{MP}_{cross,\,fib}$ as $n_l \to \infty$ which yields

$$\lim_{n_l \to \infty} \bar{n}^{MP}_{cross,\,fib} = \bar{n}_{cross,\,fib} \left(\frac{e^{-\bar{c}}}{2} \coth\left(\frac{\bar{c}}{2}\right) \left(f_f + (e^{\bar{c}} - 1) f_w + 2 f_b \sinh(\bar{c}) \right) \right). \quad (83)$$

When $f_w \approx f_b \approx 1$ and $f_f = 0$ and for typical values of $\bar{c}$ within a layer, we expect the number of crossings per fibre in a multi-planar sheet to be about two and a half times that for a 2-D network as given by Equation (79). Thus, the number of contacts per fibre in a multi-planar structure is between 0.4 and 0.6 times the aspect ratio, depending on the mean coverage per layer.

Relative bonded area

Having derived expressions for the number of contacts per fibre in 2-D and multi-planar networks, Kallmes, Corte and Bernier went on to consider the fraction of the fibre surface area which is in contact with other fibres [105]. Kallmes *et al*. considered a collapsed fibre within the body of the sheet and noted that at a given location along the fibre length precisely three contact states were possible; the fibre may be in contact with other fibres on neither surface, one surface only, or on both surfaces. Extending the 2-D model to such that the area covered by more than *three* fibres is negligible, we allow $\bar{c} \leq 0.870$. Now, the total projected fibre area per unit area is the same as the mean coverage; denoting the Poisson probability of point coverage by c fibres $P(c)$, the fraction of fibre area in contact with no other fibres say $B(0)$ is given by

$$B(0) = \frac{P(1)}{\bar{c}}$$

$$= e^{-\bar{c}} \quad (84)$$

and the fraction of fibre area in contact with one fibre is

$$B(1) = \frac{2}{\bar{c}} (1 - (P(1) + P(0)))$$

$$= \frac{2}{\bar{c}} (1 - e^{-\bar{c}} - \bar{c} e^{-\bar{c}}) \tag{85}$$

and, by definition, the fraction of fibre area in contact with two fibres is

$$\begin{aligned} B(2) &= 1 - B(0) - B(1) \\ &= 1 - \frac{2}{\bar{c}} + \left(1 + \frac{2}{\bar{c}}\right) e^{-\bar{c}} \end{aligned} \tag{86}$$

The unbonded fraction of a fibre consists of the regions covered by one fibre only, and the outermost surfaces of fibres in regions covered by two or three fibres. Thus, the fraction of a fibre which is not in contact with other fibres is $(P(1) + P(2) + P(3))/\bar{c}$ so the relative bonded area is

$$RBA = 1 - \frac{P(1) + P(2) + P(3)}{\bar{c}} \tag{87}$$

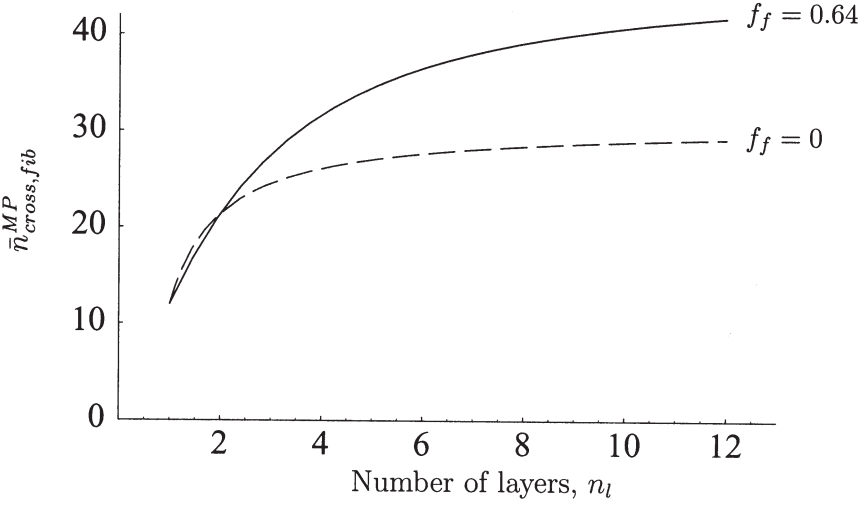

Figure 17 Number of contacts per fibre for multi-planar networks. Curves plotted using data from [104] for sulphite fibres with mean coverage in a layer $\bar{c} = 0.4$.

since we have defined the 2-D model such that $P(c > 3)$ is negligible, then $P(3) \approx (1 - P(0) - P(1) - P(2))$ and

$$RBA = 1 - \frac{(1 - P(0))}{\bar{c}}$$
$$= 1 - \frac{1 - e^{-\bar{c}}}{\bar{c}}. \tag{88}$$

Dodson points out [12] that Equation (88) gives $RBA \approx 37$ % for $\bar{c} = 1$ and plots of $B(0)$, $B(1)$ and $B(2)$ against RBA as given in *e.g.* [94, 105] are valid only up to this limit[1].

Free-fibre lengths

The expected distance between crossings or the expected *free-fibre-length* or *gap-length* follows directly from the expressions for the expected number of contacts per fibre. It is given by

$$\bar{g} = \frac{\bar{\lambda}}{\bar{n}_{cross,\,fib} - 1} \tag{89}$$
$$\approx \frac{\bar{\lambda}}{\bar{n}_{cross,\,fib}} \qquad \text{for } \bar{n}_{cross,\,fib} \gg 1 \tag{90}$$

The distribution of free-fibre lengths is given by the negative exponential distribution [90,106]; this distribution arises directly from the Poisson distribution as the probability of zero events in a given interval and has probability density function

$$f(g) = \frac{1}{\bar{g}} e^{-\frac{g}{\bar{g}}}, \tag{91}$$

with variance, $\sigma^2(g) = \bar{g}^2$.

Kallmes and Corte [90] measured the distances between fibres intersecting an arbitrary scanning line in thin laboratory formed networks, and Kallmes and Bernier [106] measured the free-fibre lengths of fibres at the surface of thicker laboratory formed sheets. In both cases, the negative exponential distribution was found to give good agreement with the data.

[1]In fact, for $\bar{c} = 0.870$, Equation (88) gives $RBA \approx 33$ %.

An important feature of the free-fibre length distribution is that it is unaffected by the width of fibres [90, 106]. The effect of increasing width is to close the smallest gaps, whilst reducing the size of larger ones. The result is given also by Miles [56] who considered the distribution of radii of circles inscribed in the polygons formed by free-fibre lengths; this is also negative exponential and the distribution is insensitive to mean fibre width and to the fibre width distribution. Naturally, this result applies strictly only in the case of infinite length fibres, however for typical fibre aspect ratios and levels of coverage, it may be applied to finite length fibres as confirmed by the results of Kallmes and co-workers discussed above [90, 106].

Void distribution

As in earlier sections, the modelling of the void distribution in fibre networks is presented here in two parts; firstly the porosity distribution and secondly the pore size distribution. The porosity distribution, *i.e*. the complement of the density distribution, is given, by analogy to the distribution of local grammage, as the distribution of local density of finite zones. From the Central Limit Theorem in statistics, we expect the distribution of local density or porosity to be Gaussian; recently Dodson and Sampson [86] proposed that the relationship between local grammage and local thickness could be modelled by a bivariate Normal distribution such that the variance of local density is given by

$$\sigma_x^2(\tilde{\rho}_{\text{net}}) = \left(\frac{\bar{\beta}}{\bar{z}}\right)^2 \left(CV_x^2(\tilde{\beta}) - \frac{2Cov_x(\tilde{\beta},\tilde{z})}{\bar{\beta}\bar{z}} + CV_x^2(\tilde{z}) \right), \tag{92}$$

where ρ_{net} is the network density, z is network thickness, $CV_x(\tilde{\beta})$ and $CV_x(\tilde{z})$ are the coefficients of variation of local grammage and thickness respectively and $Cov_x(\tilde{\beta}, \tilde{z})$ is the covariance of $\tilde{z}$ and $\tilde{\beta}$ and is given by

$$Cov_x(\tilde{\beta}, \tilde{z}) = \overline{\tilde{\beta}\tilde{z}} - \bar{\beta}\bar{z} .$$

In a subsequent publication, Dodson *et al*. [107] tested Equation (92) against experimental data and found excellent agreement for laboratory formed networks with a range of formations.

At present, Equation (92) does not allow the variance of local density to be determined analytically for random fibre networks. We have seen that the variance of local grammage may be determined analytically however, the local thickness of a zone, and hence the variance of local thickness, is

dependent not only on the local coverage but also on the vertical separation of fibres and the distribution of this property. Theory describing the pore height distribution in random networks is presented by Dodson [108] in these proceedings and measurements of pore height suggesting a negative exponential distribution are given by Niskanen *et al*. [109, 110] for simulated random structures incorporating fibre flexibility as a variable; similar distributions are reported by Holmstad and Gregersen [111] who used image analysis to measure the pore heights in paper cross-sections. The problem of combining pore height and grammage distributions to yield sheet thickness distributions remains to be solved. The recent data of Dodson *et al*. [112] shows however that there are strong correlations between the coefficients of variation of thickness and grammage for laboratory formed sheets and that the mean sheet density decreases with worsening formation.

The second class of void distribution of interest is the distribution of pore areas and pore radii. The result of Miles [56] that the radii of inscribed circles have a negative exponential distribution has already been mentioned. In the same article, Miles showed that the expected number of sides per polygon is 4 and this result was used by Kallmes and Corte [90] to derive the probability of pore areas for squares of side g where g has a negative exponential distribution. The resulting expression may be written [113]

$$g(a_p) = \frac{\sqrt{\pi}}{2\bar{g}} \frac{e^{-\frac{\sqrt{a_p}\pi}{\bar{g}}}}{\sqrt{a_p}}, \tag{93}$$

where a_p is pore area. The derivation was extended by Corte and Lloyd [113] who derived the probability density function for rectangular pores with sides drawn from independent identical negative exponential distributions such that

$$g(a_p) = \frac{2}{\bar{g}^2} K_0(\zeta) \qquad \text{where } \zeta = \frac{2\sqrt{a_p}}{\bar{g}} \tag{94}$$

and $K_0(\zeta)$ is the zeroth order modified Bessel function of the second kind.

Corte and Lloyd compared pore area distributions obtained from computer simulations of random networks with those given by Equations (93) and (94) and observed that Equation (94) gave the better approximation. Defining the polygon radius r_p as that of a circle with area equal to that of a polygon such that

$$r_p = \sqrt{\frac{a_p}{\pi}},$$

Corte and Lloyd determined the distribution of pore radii which has probability density

$$h(r_p) = \frac{4\pi r_p}{\bar{g}^2} K_0(\zeta) \qquad \text{where } \zeta = \frac{2\sqrt{\pi} r}{\bar{g}} \tag{95}$$

and the mean pore radius and variance of pore radii are given by

$$\bar{r}_p = \frac{\sqrt{\pi}\bar{g}}{4} \tag{96}$$

$$\sigma^2(r_p) = \left(\frac{1}{\pi} - \frac{\pi}{16}\right)\bar{g}^2 \tag{97}$$

respectively. An important feature of Equations (96) and (97) is that they implicitly state that in a random fibre network, the standard deviation of pore radii is proportional to the mean pore radius and that the coefficient of variation of pore radii is constant and given by $\sqrt{16 - \pi^2}/\pi \approx 0.788$. Corte and Lloyd observed also that the probability density given by Equation (95) was well approximated by the lognormal distribution. Measurements of the pore radius distribution using fluid porometry as discussed earlier were presented by Corte and Lloyd for laboratory formed sheets with differing formations, and by Bliesner [114] for laboratory formed sheets with differing grammages, show that the standard deviation of pore radius is indeed proportional to the mean; the mean pore radius decreasing with increasing grammage and improved formation. Note however that, in contrast to the relationships given above, the data of Corte and Lloyd and those of Bliesner suggest that the coefficient of variation of pore radii increases with increasing pore radii; this result is discussed further in our consideration of non-random networks.

In filtration applications, the distribution of interest is the area frequency of pore radii, because, given two circular voids of differing area, the probability of a particle encountering a given void is proportional to its area. The area frequency distribution of inscribed circles in a random fibre network has been derived by Castro and Ostoja-Starzewski [115] and is given by

$$j(r_{in}) = 4\mu_\lambda^3 r_{in}^2 \, e^{-2\mu_\lambda r_{in}}, \tag{98}$$

where r_{in} is the radius of an inscribed circle and μ_λ is the total fibre length per unit area which, from Equation (59), is given by

$$\mu_\lambda = \frac{\bar{c}}{\omega},$$

such that the area weighted mean and variance of inscribed circle radii are given by

$$\bar{r}_{in} = \frac{3}{2\mu_\lambda} = \frac{3}{2}\frac{\omega}{\bar{c}} \tag{99}$$

$$\sigma^2(r_{in}) = \frac{3}{4\mu_\lambda^2} = \frac{3}{4}\left(\frac{\omega}{\bar{c}}\right)^2. \tag{100}$$

Thus the standard deviation of inscribed circle radii is proportional to the mean inscribed circle radius and the coefficient of variation of inscribed circles is constant and equal to $1/\sqrt{3} \approx 0.577$.

Since the free-fibre length distribution is insensitive to fibre width, it follows that the pore radius distribution is also, for a given total fibre length per unit area. A further parameter of interest, which might be used to combine the pore area and porosity distributions is the expected number of pores per unit area $\bar{n}_{pore}$. This property was derived for a 2-D random network of fibres by Piekaar and Clarenburg [116] and is given by

$$\bar{n}_{pore} = \left(1 - \frac{\mu}{A}\right)\left(\frac{\mu}{\pi}(\mu - 1) - \frac{\mu}{2}\right), \tag{101}$$

where, μ is the number of fibres per unit area.

Non-random networks

As discussed previously, the structure of paper, particularly that formed on a paper machine, departs significantly from that given theoretically for random networks in two main ways. Firstly, forming consistencies are typically too high to allow fibres to remain independent in suspension and hence the sheet is formed from a flocculated network; secondly, where there is an oriented flow, fibres align themselves preferentially in the direction of flow giving rise to a nonuniform fibre orientation distribution. The interaction of fibres in flowing suspensions during the filtration process and the influence of paper-

making variables are discussed in the sequel; here we consider the modelling of non-random networks.

Fibre orientation

The interaction between fibres in suspension and the influence of forming section hydrodynamics on the fibre orientation distribution in paper are discussed by Niskanen [4] and several of the more common functions used in the modelling of fibre orientation effects are given by Mark [13] and Schaffnit [102]. Here, the probability densities for some of these functions are given and compared; functions are given here in a form such that the maximum and mean fibre orientation occurs at an angle of $\pi/2$, *i.e.* the machine direction; where the maximum orientation occurs at an angle $\pm\psi$ to the machine direction, parameter θ in Equations (102, 105) and (106) to (108) should be replaced by $(\theta \pm \psi)$.

- The Cosine distribution has probability density given by

$$s(\theta) = \frac{1}{\pi}\left(1 - \epsilon_1 \cos(2\theta) - \epsilon_2 \cos(4\theta) - \ldots - \epsilon_n \cos(2n\theta)\right) \tag{102}$$

where $0 \leq \epsilon_1, \epsilon_2 \ldots, \epsilon_n \leq 1$ and the variance is given by

$$\sigma^2(\theta) = \frac{\pi^2}{12} - \frac{\pi}{2}\epsilon_1 - \frac{\pi}{8}\epsilon_2 - \ldots - \frac{\pi}{2n^2}\epsilon_n \tag{103}$$

and the orientation ratio is given by

$$\frac{s(\pi/2)}{s(0)} = \frac{\pi(-\epsilon_1 + \epsilon_2 - \epsilon_3 + \ldots) - 1}{\pi(\epsilon_1 + \epsilon_2 + \epsilon_3 + \ldots) - 1} \tag{104}$$

Often the function is truncated for ease of manipulation such that

$$s(\theta) = \frac{1}{\pi}\left(1 - \epsilon \cos(2\theta)\right) \tag{105}$$

which has variance $\sigma^2(\theta) = \frac{\pi^2}{12} - \frac{\pi}{2}\epsilon$ and orientation ratio $\frac{1 + \pi\epsilon}{1 - \pi\epsilon}$

- The von Mises distribution has probability density given by

$$s(\theta) = \frac{1}{\pi I_0(\epsilon_{vm})} \epsilon^{-e_{vm}\cos(2\theta)} \tag{106}$$

where $I_0(\epsilon_{vm})$ is the zeroth order modified Bessel function of the first kind. The variance must be determined by numerical integration using

$$\sigma^2(\theta) = \int_0^{\pi} \theta^2 \, s(\theta) \, d\theta - \frac{\pi^2}{4},$$

and the orientation ratio is $e^{2\epsilon_{vm}}$.

- The elliptical distribution has probability density

$$s(\theta) = \frac{l_\epsilon}{\pi} \frac{1}{l_\epsilon^2 \cos^2(\theta) + \sin^2(\theta)} \qquad \text{for } l_\epsilon > 1\,. \tag{107}$$

Again the variance must be determined by numerical methods; the orientation ratio is l_ϵ^2.

- The wrapped Cauchy distribution has probability density

$$s(\theta) = \frac{1}{\pi} \frac{1 - \epsilon_c^2}{1 + \epsilon_c^2 + 2\epsilon_c \cos(2\theta)}. \tag{108}$$

The variance must be determined by numerical integration and the orientation ratio is $\dfrac{(\epsilon_c + 1)^2}{(\epsilon_c - 1)^2}$.

It turns out that the elliptic and wrapped Cauchy distributions are identical at a given orientation ratio, *i.e.* substitution of $l = \dfrac{\epsilon_c + 1}{\epsilon_c - 1}$ into Equation (107) yields, on simplification, Equation (108). Figure 18 shows the fibre orientation distributions for the single-parameter cosine, von Mises and the wrapped Cauchy/elliptical distributions, at an orientation ratio of 3:1; the coefficient of variation of fibre orientation angle is plotted against orientation ratio for these three functions in Figure 19. It is readily apparent that the coefficient of variation of fibre orientation is only weakly dependent on the orientation ratio and is influenced only slightly by the choice of distribution function. Note also that for a *uniform* fibre orientation distribution as applied to

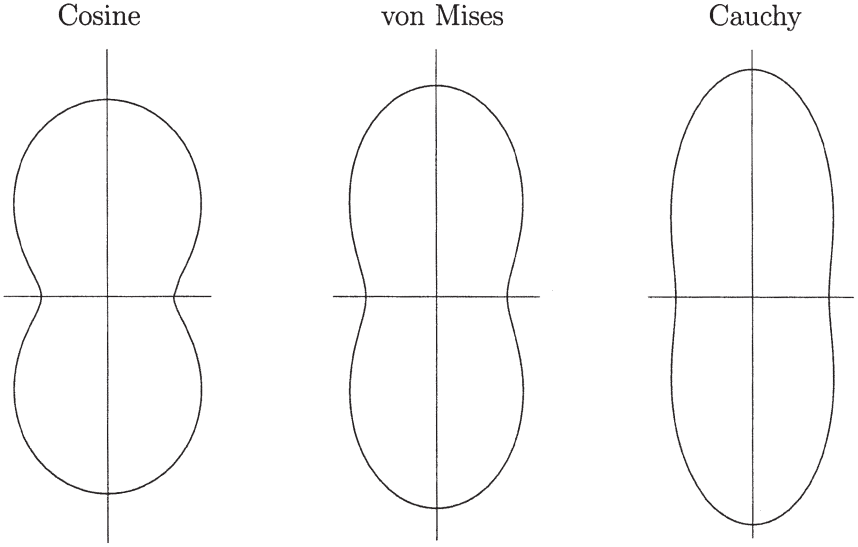

Figure 18 Comparison of functions describing fibre orientation distribution at orientation ratio 3:1.

random networks, $s(\theta) = 1/\pi$, the variance $\sigma^2(\theta) = \pi/12$ and the orientation ratio is 1.

The effect of a fibre orientation distribution on the distribution of mass density in networks with randomly positioned fibre centres was investigated by Dodson and Fekih [117] who derived the autocorrelation coefficient for fibres oriented with probability density given by a one parameter cosine distribution. A 2:1 fibre orientation ratio was shown to increase the coefficient of variation of local grammage for square inspection zones by around 14 % relative to that given for a random network of the same fibres with a uniform distribution of orientations.

Schaffnit and Dodson [118] noted that the experimental results of Waterhouse [44] and the simulation data of Cresson [119] both showed little or no influence of fibre orientation distribution on the distribution of local grammage and therefore disagreed with the theoretical result of Dodson and Fekih [117] discussed above. Schaffnit and Dodson derived the autocorrelation function, and hence the fractional between zones variance for fibres with axes orientations given by the one-parameter cosine distribution, the wrapped Cauchy distribution and a rectangular distribution. The resulting

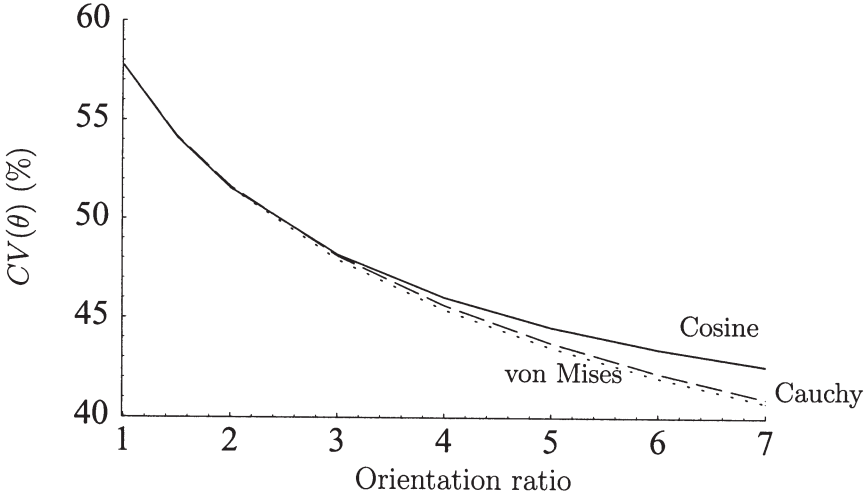

Figure 19 Coefficient of variation of fibre orientation plotted against orientation ratio.

expressions and computations showed the distribution of mass density to be insensitive to fibre orientation for the one parameter cosine distribution, to be negligibly less uniform with increasing orientation for the wrapped Cauchy distribution and to be slightly more uniform with increasing orientation for the rectangular distribution. In conclusion, Schaffnit and Dodson considered the distribution of mass density to be only slightly influenced, if at all, by the degree of fibre orientation; the result of Dodson and Fekih [117] was identified as being attributable to an approximation in the derivation. Schaffnit and Dodson showed also that the introduction of an additional term in the cosine distribution had a negligible effect on the distribution of mass density. It should be noted however that in commercially formed networks, fibre orientation is influenced by forming section hydrodynamics, which in turn influence formation and these effects may well be coupled, see *e.g.* [120].

The findings of Schaffnit and Dodson [118] were confirmed in a simulation study by Soszynski [121] who computed the fractional between zones variance for networks of rectangular fibres with randomly located fibre centres and with axes oriented with probability density given by a two parameter cosine distribution

$$s(\theta) = \frac{1}{\pi} + \frac{\cos(2\theta)}{\pi} + \frac{\cos(4\theta)}{2\pi}. \tag{109}$$

such that the orientation ratio was 5:1. Soszynski found that for square inspection zones, the fractional between zones variance was insensitive to the orientation of fibres. For rectangular inspection zones however, the fractional between zones variance was dependent on fibre orientation.

Corte and Kallmes [73] note that a preferential fibre orientation reduces the mean number of contacts per fibre and hence increases the mean free fibre length and the mean polygon area but decreases the number of polygons per unit area. In contrast, Castro and Ostoja-Starzewski [115], state that the number of polygons per unit area and the area-frequency of inscribed circle radii is insensitive to the fibre orientation distribution. Kallmes and Bernier [122] note that increased fibre orientation introduces a similar Relative Bonded Area distribution but does not affect the relative fractions of fibre areas in contact with 0, 1, or 2 fibres as given by Equations (84) to (86); this is perhaps unsurprising since these expressions are functions of the mean coverage only.

Flocculation

A requirement of modelling the structure of flocculated networks is that the location of each fibre is no longer independent of the location of other fibres; nevertheless, the inherent stochasticity of the structure must be retained. The first approach to this problem was presented by Corte and Kallmes [73] who considered a 2D structure of randomly placed circles of uniform radius; areas covered by circles were assumed to contain a number of points drawn from a Poisson distribution, and areas not covered by circles were assumed to contain points drawn from another Poisson distribution with smaller mean. The parameter modelled was the distribution of the number of points per unit area, which, for sufficiently large zones, is proportional to the distribution of local grammage. Kallmes and Bernier [122] simulated flocculation by generating a random array of fibre centres within an area and subdividing the area into square zones and then calculating the centre of gravity of each zone. Fibre centres within each zone were then moved towards or away from the centre of gravity of that zone to generate 'positively flocculated' or 'negatively flocculated', *i.e*. disperse, structures respectively.

In a simulation study, Gorres *et al*. [123] generated images of flocculated networks by specifying circular regions with randomly located centres in a plane and placing n_{floc} fibres, modelled as rectangles, with centres distributed randomly within these circular regions. Gorres *et al*. varied the number of

fibres within such a floc and the diameter of the circular regions to vary floc density. The results showed worsening formation was associated with an increase in the number of fibres per floc and the autocorrelation coefficient was approximately proportional to the logarithm of floc density. Gorres *et al*. simulated also the random deposition of solid disks with the same radii and densities used for the floc deposition model; the results indicated that the formation of the sheet was largely insensitive to the choice of fibre or disk model at high floc densities but was highly sensitive at lower floc densities.

An analytic approach to a similar problem was given by Deng and Dodson [124] who noted that the formation number $n_{f,x}$, defined previously, if constant, represents approximately the number of fibres in a clump which, if dropped at random, would have exhibited the same structural variability. Noting that experimental measurements of $n_{f,x}$ made on commercial papers show a proportional dependence on zone size, Deng and Dodson derived the autocorrelation function for regular stars with n_s arms, *i.e*. representations of 'hard-centred' flocs formed from n_s fibres with all fibres in a star crossing at the fibre centre; the full derivation is given in Chapter 3 of [12]. Whilst the variability observed in a given sample could be reproduced at a given inspection zone size using the star model, the calculated values of $n_{f,x}$ were constant; Deng and Dodson attributed the difference to the fact that real flocs are not hard-centred and cooperative drainage effects, as proposed by Wrist [125], may act upon flocs in the sheet forming process.

An analytic approach to modelling planar flocculated structures was presented by Farnood and co-workers [126, 127] who derived the variance of local grammage of a network of low-grammage disks with and without a distribution of diameters. Farnood *et al*. found that the decay of variance with zone size found in commercially formed papers could be achieved also by the random deposition of such disks with uniform grammage and a log-normal distribution of disk radii; though for small inspection zone sizes the approximation given by uniform sized disks was also excellent. For a structure made from disks of mean diameter $\bar{D}$ and mean grammage $\bar{G}$, the variance of local grammage using square zones of side length x is approximated by

$$\sigma_x^2(\tilde{\beta}) \approx \bar{\beta}\bar{G}(1 - \frac{2x}{\pi\bar{D}} + \ldots) \qquad \text{for } x \leq \bar{D}\,. \tag{110}$$

Equation (110) may be derived from the formulae given on pages 97–99 of [12] and a similar expression, arrived at by numerical methods is given by Farnood [126]. Since the uniform size disk model gives good agreement at small inspection zone sizes, parameters $\bar{G}$ and $\bar{D}$ can be determined from

measurements of variance at small scales. Since the point variance for a random structure of disks is given by

$$\sigma^2(\beta) = \bar{\beta}\bar{G}, \tag{111}$$

then $\bar{G}$ may be calculated by extrapolating small scale variance data to determine the variance at points. In practice this is best achieved by taking the logarithm of local variance plotted against zone size, which is approximately linear at small scales of inspection. Knowing $\bar{G}$, $\bar{D}$ may be calculated from the differential form of Equation (110)

$$\frac{d(\sigma_x^2(\tilde{\beta}))}{dx} = -\frac{2\bar{\beta}\bar{G}}{\pi\bar{D}} \qquad \text{for } x \le \bar{D} \tag{112}$$

In an analysis of 130 machine-made and laboratory formed papers, including 22 reported by Corte [95], Farnood and Dodson [128] reported a coefficient of determination of 0.99 for the correlation

$$\sigma(D) = 1.2\bar{D}^{\frac{2}{3}} \tag{113}$$

for lognormal distributions of disk diameters. A subset of these data[1], given in an appendix to [126], is plotted in Figure 20. The result, termed the *similarity law of formation* by Farnood and Dodson [128] is important since the data on which the regression was performed span 25 years of papermaking and the correlation is applicable across a range of commercial and laboratory forming mechanisms. Since the standard deviation of disk diameters is so closely correlated to the mean disk diameter, sheet structures may be quantified by two independent parameters, namely the mean disk grammage $\bar{G}$ and the mean disk diameter $\bar{D}$ which correspond to the intensity and scale of mass distribution respectively [126, 127, 128]. In a subsequent simulation study, Farnood *et al*. [129], generated a graphical 'formation diagram', allowing rapid semi-quantitative assessment of the formation of a sample by comparison with the images.

Void distribution

It was shown in the discussion of random networks that the distribution of density could be described via the bivariate Normal relationship between

[1]Note that data for sample numbers 64 to 72 and 96, given in the appendix to [126] are not plotted in Figure 20 since these data arise from analysis of simulated structures.

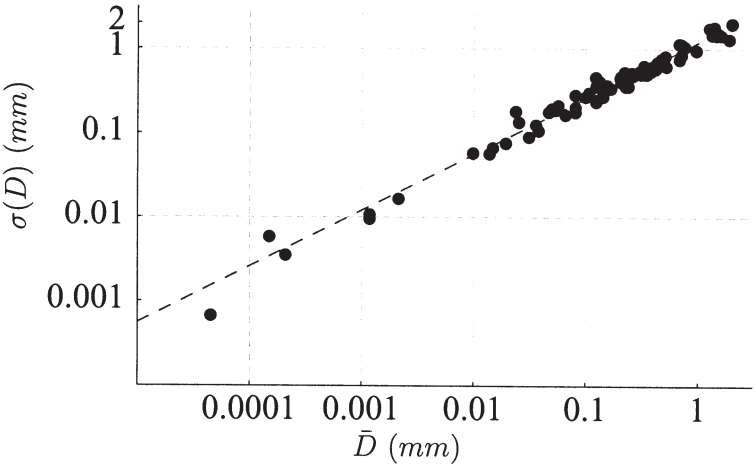

Figure 20 Relationship between mean and standard deviation of floc diameter. Data from Farnood [126]; broken line has gradient 1.2 as given by Equation (113).

local thickness and local grammage in the network [86]; Equation (92) states that the variance of density at a given scale of inspection is given by the coefficients of variation of local grammage and thickness and their covariance. For flocculated structures, the coefficient of variation of local grammage may be estimated via the disk model of Farnood *et al.* [126, 127, 128]; however, as noted for random structures, analytic expressions for the variance of thickness or the covariance of local thickness and grammage are not yet available. Nevertheless, the experimental data of Dodson *et al.* [107] show that Equation (92) holds equally well for sheets with approximately random structures as for highly flocculated sheets. The measurements presented in [107] were made on sheets pressed at the standard laboratory pressure of 345 *kPa* (50 *psi*) and it is likely that the higher pressures encountered in the manufacture of machine-made papers will result in departure of the local thickness-grammage relationship from bivariate Normal. This remains to be verified by future experimental work which should indicate the appropriate direction for subsequent modelling studies.

We have noted already the agreement observed by Corte and Lloyd [113] between their model of the pore radius distribution in random networks and measurements made on flocculated sheets; both theory and experiment suggesting that the standard deviation of pore radii was proportional to the mean pore radius. Dodson and Sampson [130] noted that this agreement was

surprising since, by their very design, the sheets prepared by Corte and Lloyd were manifestly non-random. Now, Corte and Lloyd's derivation used the established analytic result that the distribution of free-fibre lengths in a *random* network is negative exponential. Neither experimental measurements nor the equivalent analytic result exist for flocculated networks. Dodson and Sampson noted however that in a flocculated sheet, dense regions will consist of several small free-fibre lengths and sparse regions will consist of fewer, larger free-fibre lengths, giving rise to the expectation that the free-fibre length distribution in a flocculated network will exhibit a positive skew and a greater variance than that in a random network. Also, the results of simulations by Scharcanski and Dodson [131] suggested that the free-fibre length distribution in flocculated networks could be approximated by a family of gamma distributions which exhibit a positive skew.

Accordingly, Dodson and Sampson [130, 132] rederived the theory of Corte and Lloyd [113] using the gamma distribution to describe the free-fibre length distribution. The gamma distribution has probability density given by

$$f(g) = \frac{b^k}{\Gamma(k)}\, g^{k-1}\, e^{-bg} \tag{114}$$

with mean $\bar{g} = k/b$ and variance $\sigma^2(g) = k/b^2$. Note that the negative exponential distribution is a special case of the gamma distribution such that when $k = 1$, Equation (114) recovers Equation (91) with $\bar{g}_{rand} = 1/b$.

Dodson and Sampson [130] derived the probability density of pore areas as

$$g(a_p) = \frac{2\, a_p^{\,k-1} b^{2k} K_0(\zeta)}{\Gamma(k)^2}\,, \qquad \text{where } \zeta = 2b\sqrt{a_p} \tag{115}$$

and $K_0(\zeta)$ is the zeroth order modified Bessel function of the second kind.

The probability density of pore radii was given by Dodson and Sampson as

$$h(r_p) = \frac{4 b^{2k} \pi^k r_p^{2k-1} K_0(\zeta)}{\Gamma(k)^2}, \qquad \text{where } \zeta = 2b r_p \sqrt{\pi}. \tag{116}$$

The mean and variance and coefficient of variation of $h(r_p)$ are given by:

$$\bar{r}_p = \frac{\Gamma(k+\tfrac{1}{2})^2}{b\sqrt{\pi}\Gamma(k)^2} \tag{117}$$

$$\sigma^2(r_p) = \bar{r}_p^2 \left(\frac{k^2 \Gamma(k)^4}{\Gamma(k+\tfrac{1}{2})^4} - 1 \right) \tag{118}$$

$$CV(r_p) = \sqrt{\frac{k^2\Gamma(k)^4}{\Gamma(k+\frac{1}{2})^4} - 1} \tag{119}$$

respectively. An important feature of the model is that we have the analytic result that when $k = 1$, Equations (115) to (118) recover Equations (94) to (97). Thus, we have a unified model for the pore radius distribution in random and nonrandom networks; the random case existing as a 1-parameter special case of the 2-parameter family of distributions. In fact, the probability density function given by Equation (116) is itself well approximated by a gamma distribution with $k \mapsto \frac{1}{2}((16k^2 + 1)^{\frac{1}{2}} - 1)$ and $b \mapsto 2b\sqrt{\pi}$ [133].

Dodson and Sampson [130] found good agreement between the pore radius distribution given by Equation (116) and the lognormal distributions reported by Corte and Lloyd [113] and Bliesner [114]. They calculated also parameters k and b for these data, and found that these exhibited an affine relationship when plotted against each other; both k and b increasing with grammage and decreasing with worsening formation.

As yet, the theory of Dodson and Sampson does not provide any insights into the observed proportionality between the standard deviation of pore radii and the mean pore radius observed by Corte and Lloyd [113] and Bliesner [114]. Good agreement has been shown however between this theory and experimental data [134] and it has the benefit of incorporating random networks as a special case. Note also that the gamma distribution has been found to accurately describe the pore radius distribution in a range of stochastic porous media including fibrous filters, granular beds and sintered metal plates, see *e.g.* [135, 136, 137].

Recently, Sampson [133] has argued that, since pore radii are real and positive then any plot of the standard deviation of pore radii against the mean pore radius should pass through the origin; it follows directly that if this relationship is linear then the coefficient of variation of pore radii is constant and equal to the gradient of the plot. Experimental data for fibres of differing lengths and coarseness, but of similar width, presented in [133] is given in Figure 21; there are two important features which are being incorporated into ongoing theoretical studies at UMIST. Firstly, the effects of changing grammage and formation cause the standard deviation and the mean to move along the same line, and secondly, the intercept with the ordinate is close to zero, indicating that the coefficient of variation of pore radii is, at least to a first approximation, independent of the grammage and formation of the sheet.

The pore radius distribution models of Corte and Lloyd [113] and Dodson and Sampson [130] depend directly on the free-fibre length distribution. Indeed, Dodson and Sampson [130] used their theory to back-calculate the

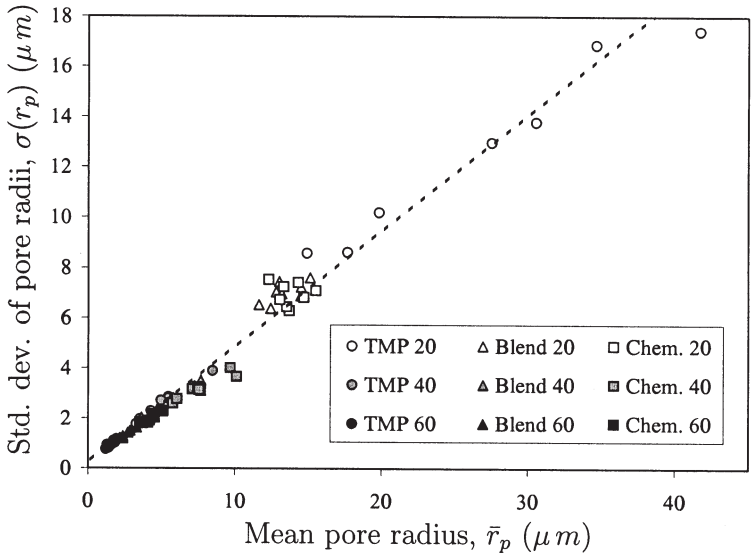

Figure 21 Standard deviation of pore radii plotted against mean pore radius. Data shown is for laboratory formed sheets with nominal grammages 20, 40, and 60 $g\ m^{-2}$ and a range of formations formed from TMP, Chemical softwood and a 1:1 blend of the two pulps.

free-fibre length distribution from the pore size data of Corte and Lloyd. Since the free-fibre length distribution is determined to some extent by the fibre orientation distribution [73] then we expect also a dependence of the void structure on the fibre orientation distribution; also, the recent simulation results of Kim and Pourdeyhimi [138] show the mean pore area to increase with increasing anisotropy. The dependence of void structure on anisotropy has been modelled by Silvy [139] who defines an *equivalent pore* as a polar representation of the length-weighted orientation distributions of fibre segments which is 'equivalent' to the mean shape of voids within the sheet [13]. Thus the equivalent pore is the contour $\mathcal{E}$ obtained in the plane of the sheet by cumulatively placing fibre segments end to end whilst maintaining their orientation [102] where the radius of curvature at a given angle θ is given by

$$R(\theta) = \frac{dL_\theta}{d\theta} \tag{120}$$

where L_θ is the cumulative length of fibre segments projected onto the plane whose orientations lie between θ and $\theta + \Delta\theta$. The length weighted orientation distribution is given by

$$n_{l\theta} = \frac{1}{\mathcal{L}} R(\theta) \tag{121}$$

where $\mathcal{L}$ is the cumulative length of all fibre segments in the network and the perimeter of the contour $\mathcal{E}$ is $2\,\mathcal{L}$.

FLOCCULATION AND SHEET FORMING DYNAMICS

The structural characteristics of the fibre suspension from which a sheet is formed will influence those of the formed sheet. A thorough overview of the physics of forming is given by Norman [140, 141] who, with Söderberg, contributes also a review on the subject of forming to this symposium. The mechanics of fibre flocculation and dispersion have been studied extensively by Kerekes and co-workers and are reviewed in [2, 72, 142]. It is not the purpose of this article to repeat the material in these reviews; it is important to note however that the extent of flocculation in the network is influenced by the presence of turbulent eddies, their scale and their rate of decay through the associated shear forces acting upon fibres. The design of headboxes and dewatering elements involves consideration of such flows and the development of flow geometries to optimise dispersion. The relationship between the scale of eddies and floc evolution and rupture is discussed and modelled by Steen [143, 144, 145] and expressions relating fibre geometry and flexibility to floc strength are given by Kerekes [142], Farnood *et al*. [146] and Andersson *et al*. [147]. Here, observations relating the structure of suspensions to those observed in the formed sheet are discussed. Whilst recognising the importance of chemical additives to the flocculation propensity of fibre suspensions, a result given by Chatterjee [148] greatly simplifies the analysis. Chatterjee studied the effects of chemical flocculants and increased suspension consistency, *i.e*. increased potential for mechanical flocculation, and concluded that their effects on the distribution of mass density of formed sheets were not easily distinguished. It seems therefore the interaction of fibres in suspension generates a similar class of flocculated structures, whether promoted by chemical or physical means.

As we have seen in the discussion of fibre orientation distributions, oriented flow and a jet to wire speed difference introduce oriented shear in the

forming section which in turn generates a fibre orientation distribution. Niskanen observed that the shape of the resulting distribution was sensitive to the flexibility of fibres in suspension; flexible fibres adjusting to shear forces by bending along their length whilst stiffer fibres adjust by rotation [4]. The orientation of *flocs* has been studied by Praast and Göttsching [120] who measured the orientation of local gradients of light transmission images; the technique is similar to that described by Scharcanski and Dodson [149, 150] who reported good agreement of measurements of spatial anisotropy made on light transmission images and grammage distributions taken from β-radiographs. Praast and Göttsching [120] observed good correlations between the average orientation of flocs and that of fibres; both properties exhibiting similar profiles in the cross-machine direction. A secondary orientation effect was demonstrated for Fourdrinier formed papers by Finger and Majewski [151] who found that fibres had a small but appreciable orientation to the plane of the sheet.

Given a sufficiently dilute suspension, say in the chamber of a laboratory sheet former, the structure of the formed sheet exhibits a similar variability to a random network [12, 102] and the measured influence of changing fibre length and coarseness is broadly in line with theoretical expectation [152, 153]. In commercial forming processes, the interaction of fibres results in a floc size distribution in the suspension. The measurements of Hourani [154, 155] and those of Karema *et al*. [20, 21] suggest that this distribution is approximately lognormal, *i.e*. has a positive skew and a long tail. The data of Hourani [155] is plotted in Figure 22. Farnood [126] compared the data plotted in Figure 22 for flocs in suspension with those plotted in Figure 20 for sheets. The regression represented by the broken line in Figure 22 is that given by Farnood and is given by

$$\sigma(D) = 0.807\bar{D}^{1.246} \tag{122}$$

with a coefficient of determination of 0.96. Noting the similarity between Equations (122) and (113) Farnood attributes the different coefficient and exponent of $\bar{D}$ to the resolution of Hourani's measurements, *i.e*. 0.3 *mm*, and the fact that the analysis of radiographs which yielded Equation (113) considers also mass variability within flocs which Hourani's data does not. The solid line in Figure 22 represents a 1:1 relationship and Farnood noted that truncation of the lognormal distribution using the resolution of Hourani's measurements gives such a relationship between the standard deviation and the mean. This relationship was studied by Raghem-Moayed and Dodson [156] who modelled the evolution of flocs using a gamma distribution to parameterize random walks in three dimensions. For their parameter of floc

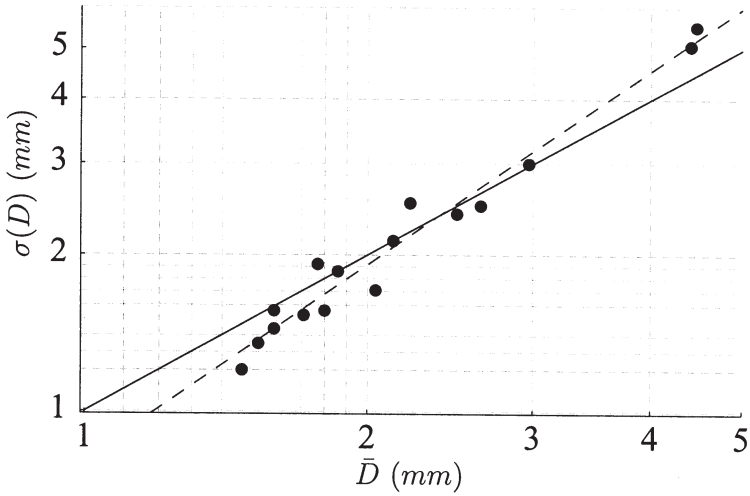

Figure 22 Relationship between mean and standard deviation of floc diameter. Data from Hourani [155]; broken line represents regression on the data, solid line represents 1:1 relationship.

size X, Raghem-Moayed and Dodson showed the standard deviation of floc size to be related to the mean according to:

$$\sigma(X) = 1.24\bar{X}^{0.67} \tag{123}$$

Equation (123) coincides with the empirical 'similarity law of formation' given by Equation (113) and therefore strongly supports the use of the lognormal distribution to represent floc sizes and the use of the gamma distribution to represent the distances between fibre crossings.

The data of Hourani, those of Farnood and the analysis of Raghem-Moayed and Dodson indicate a strong relationship between the structural characteristics of a fibre suspension and those of sheets formed by filtration of such a suspension. Further evidence of such relationships is provided by Dodson and Schaffnit [157] who examined the data of Corte [95] and observed that the formation number at the 1 *mm* scale of inspection as given by Equation (71) was correlated to the crowding number in the headbox as given by Equation (4) and mean fibre length according to the expression

$$n_{f,1} = 2.6 + 0.13\, n_{crowd} - 1.34\bar{\lambda}. \tag{124}$$

Log-linear regression on the same data was presented by Deng and Dodson [124] who found

$$n_{f,1} = e^{1.26 + 0.0253 n_{crowd} - 0.0125 °\mathrm{SR}} \tag{125}$$

$$= e^{0.721 + 0.0396 n_{crowd} - 0.161 \bar{\lambda}}, \tag{126}$$

where °SR is the Schopper-Riegler wetness of the pulp. Kiviranta and Dodson [158] investigated the relationship between formation, headbox crowding and table activity on 141 sheets formed on a pilot Fourdrinier machine. They observed the following correlation:

$$n_{f,1} = e^{0.715 + 0.025 n_{crowd} - 0.375\ T_A}, \tag{127}$$

where T_A is a measure of the table activity through measurements of forming table surface roughness obtained via image analysis and discussed by Kiviranta and Paulapuro [159]. It is instructive to compare Equations (125) to (127); whilst the third variable in the exponent differs between the analyses, the coefficient of n_{crowd} is remarkably stable over the quarter of a century which elapsed between the acquisition of data by Corte and by Kiviranta and Dodson. These relationships do not provide any insights into the physical processes occurring during the filtration of a flocculated suspension to form a sheet. Nevertheless, the existence of a correlation between indices quantifying flocculation propensity in suspension and flocculation in the sheet, and its stability over time, provides a useful basis for formation control through informed fibre preparation.

The interaction between flocs in suspension, the structure of the initial layers formed by its filtration, and the interaction between the forming structure and the arriving suspension was discussed by Wrist [125]. Wrist argued that a consequence of the lower resistance to flow of low grammage regions in the evolving network structure was that fibre would be preferentially deposited in these regions. The concept seems intuitively correct, yet it is well established that the variance of local grammage in real papers is typically greater than that calculated for random networks at scales of inspection similar to a fibre length, *i.e.* $n_{f,\bar{\lambda}} \geq 1$ [12, 95]. There is some evidence however that at small scales of inspection, the variance of local grammage may be less than for a random network [99, 100, 140]. These results suggest that the preferential drainage effect proposed by Wrist may even out the grammage distribution at small scales of inspection. The effect was studied in a simulation by Gorres *et al*. [160] who assumed that fibre ends were drawn preferentially to sparse regions in a simulated network; the results showed the expected

reduction in the variance of local grammage for a network formed with preferential drainage when compared with random network; also, the effect was more pronounced for short fibre furnishes. It should be noted that the simulations of Gorres *et al*. [160] consider only the deposition of single fibres and not of flocs.

Experimental evidence for the existence of a preferential drainage effect was presented by Sampson *et al*. [161] who investigated the evolution of the mass distribution in laboratory formed networks by testing a 1-parameter model previously proposed by Dodson [93]. The results of Sampson *et al*. showed preferential drainage effects to occur in the filtration of dilute suspensions, *i.e*. those with $n_{crowd} \approx 1$, and flocculated suspensions. The results showed also that since the initial structure of flocculated suspensions was more nonuniform than for dilute suspensions, the preferential drainage effect was stronger, though the net effect of flocculation dominated that of preferential drainage resulting in a nonuniform network. For suspensions with n_{crowd} up to about 12, the correlation

$$n_{f,1} = 44 \frac{n_{crowd}}{\bar{\beta}} \tag{128}$$

was found to give good agreement for $4\ g\ m^{-2} \leq \bar{\beta} \leq 50\ g\ m^{-2}$. The preferential drainage effect has been illustrated also for isotropic and anisotropic laboratory formed sheets by Norman *et al*. [162]. Sampson *et al*. noted that the identification of preferential drainage in the forming of laboratory sheets from dilute suspensions means that whilst such sheets exhibit similar properties to random networks, the fact that there is an interaction between arriving fibres and the previously formed structure means that structural evolution is a non-random process. Further evidence of preferential drainage is given by Lucisano and Norman [163] who inhibited fibre settling and fibre interaction by modifying the viscosity of the suspending medium and the surface charge of fibres and observed improved network uniformity with increased drainage rate.

It is worth noting finally the forming mechanism described by Radvan and Gatward [164] involving the suspension of fibres in foam and delivery of the suspension onto a modified Fourdrinier former. The system allowed good dispersion of the fibres *in suspension* and the resulting sheets exhibited good uniformity.

CONCLUSIONS

In conclusion, the material presented within this review is summarised and a group of open problems are identified.

Flocculation in suspensions

Papermaking involves the processing of inherently variable raw materials to develop physical and mechanical properties whilst minimising the persisting variability in the final product. A major source of variability in the sheet stems from the propensity of fibres to interact in suspension which gives rise to flocculated structures that influence the structural nonuniformity of the sheet formed from the filtration of a suspension. The propensity of a suspension to flocculate is influenced by its consistency and the morphology of its constituent fibres. The concept of the crowding number, calculated using average values of fibre geometries, has been presented and this seems to provide a sound dimensionless quantifier of flocculation propensity; recent theoretical developments have allowed the influence of a lognormal fibre length distribution, which is typical of many papermaking furnishes, to be incorporated in the determination of the crowding number.

Statistical characterisation

The measurement of structural nonuniformity in suspensions and in sheets has been discussed along with the appropriate statistical quantifiers of this nonuniformity. For unbonded structures such as fibre suspensions, and lightly bonded structures such as uncalendered sheets formed from unbeaten fibres, light transmission techniques allow rapid assessment of mass distribution. For typical furnishes however, the degree of bonding and its distribution means that radiographic techniques are significantly more informative. The equivalence of the two most widely used techniques for quantifying scales of variability in sheets, *viz*. the decay of the variance of local grammage with inspection zone size and the power spectrum, has been illustrated using orthotropic bandpass filtering.

Statistical geometry of random networks

The use of statistical geometry to determine properties of two- and three-dimensional fibre networks has been presented. Models for three dimensional networks have considered random networks and allow determination of the number of contacts per fibre and the variance of porosity which depend on

fibre geometry through the aspect ratio and fibre width respectively. The distribution of local grammage in two dimensional random fibre networks is known analytically and techniques for determining this property for given fibre geometries and their distribution have been compared. The equations for determining the distribution of local grammage using the line method have been stated correctly and a graphical representation has been presented which allows its rapid determination knowing fibre length and coarseness. Also of importance is the pore size distribution of a random network and this depends on the distribution of distances between fibre crossings.

Departures from randomness

The properties of random networks provide the basis for comparison when quantifying the properties of real sheets. Experimental and theoretical studies have shown that the distribution of local grammage is insensitive to changes in the fibre orientation distribution, though increased orientation increases the mean pore radius. Naturally, flocculation increases mass variability and this has been modelled as the deposition of fibre clumps and the deposition of sparse disks. The latter approach has revealed a remarkable stability in the classes of structures realised in paper-making processes in that the standard deviation of disk diameters is proportional to the mean disk diameter raised to the power $\frac{2}{3}$. A similar relationship has been observed in experimental observations of flocculated suspensions and has been derived analytically.

Forming dynamics

Another type of structural stability has emerged from experimental and theoretical studies of the pore size distribution in sheets. Here, the standard deviation of pore radius is proportional to the mean pore radius and the coefficient of variation of pore radii is, at least to a first approximation, constant for changes in sheet grammage and flocculation. During forming, the evolution of the pore structure is directly coupled with the evolution of the mass distribution. This has been demonstrated through laboratory experiments which have revealed that fibres are drawn preferentially towards sparse regions in the evolving structure, which have a lower resistance to flow than dense regions. The effect however is not sufficiently strong to overcome the effects of flocculation and at scales of inspection around a fibre length, the measured variance of local grammage is typically greater than that of a random network of the same constituent fibres.

Important open problems

We conclude by identifying several open problems which present opportunities for theoretical and experimental study, of varying difficulty:

1. **Variance of density in near-planar random networks.** As mentioned previously, the well established analytic result for the variance of grammage in random fibre networks should be combined with new theory for the pore height distribution. The pore height distribution is dependent on fibre geometry through the thickness of fibres and the grammage distribution is dependent on fibre length, width and coarseness. Thus we expect the density distribution for random networks to be defined in terms of these fibre properties.
2. **Influence of fibre length distribution on the number of contacts per fibre.** The derivation of the expected number of contacts per fibre in 3D networks is based on the concept of the crowding number. As we have seen, expressions for the influence of a lognormal fibre length distribution on the crowding number have recently been derived. Derivation of the number of contacts per fibre on this basis would allow the distribution of the number of contacts per fibre to be determined.
3. **Contact area distribution.** The study of the number of contacts per fibre is of importance in the study of network rheology. Also of importance is the area of regions of contact; in three dimensions contact area will influence the frictional forces to be overcome in disrupting a network and in two dimensions the contact area will influence the available area for inter-fibre bonding. Incorporation of fibre orientation distributions and fibre flexibility would be desirable.
4. **Statistical model for volume frequency pore size distribution.** The geometric models describing the pore size distribution in sheets give good agreement with measurements made using fluid porometry. Both models and measurements yield the number frequency of pores. Whilst simulation based models exist to describe porosimetric measurements using *e.g.* mercury intrusion techniques, statistical models for these volume frequency pore radii distributions have yet to be derived, though in a random assemblage we would expect an exponential distribution of void volumes to be a good first approximation. Such models should aim to combine the probabilities of pore radii and the pore volumes associated with them. It is likely that appropriate distribution for pore radii is the gamma distribution; pore volumes might be modelled as spheres or cubes with a given distribution of radii or side lengths respectively.

5. **Influence of fines on variance of local grammage in random networks.** It is typical to assume that fines are distributed uniformly in the plane of the sheet when determining the variance of local grammage in random networks. Thus, the fractional between zones variance is less than that for a furnish without fines by a factor (1 – fines fraction). However, it is likely that a substantial portion of fine material becomes re-attached to fibre surfaces. Naturally, fines retained in such a manner will not be uniformly distributed in the plane of the sheet and instead will act to increase mean fibre coarseness and width, thus we expect a higher variance than obtained for a uniform distribution of fines. Consideration of simple fibre cross-sectional geometries and the effect of fines attached to their surfaces on their dimensions will allow improved determination of the variance of local grammage for furnishes containing fines.
6. **Development of a variance ratio for 3D networks.** We have seen that the variance of local volumetric concentration in random 3D networks is dependent on the fibre width for cubic inspection volumes. This analytic result should be extended to yield expressions for the variance of local mass consistency which would allow appropriate measurements of the same property made on suspensions to be expressed in terms of a variance ratio allowing comparison of real and random networks similar to that given by the formation number for sheets. Coupled with estimates of suspension crowding, such a variance ratio should allow improved insights into the relationship between suspension and sheet uniformity.
7. **Distribution of optical properties.** The solution to Problem 1. should provide insights into the distribution of optical properties in random networks. Naturally, these will be influenced by the intrinsic light scattering and absorption coefficients of the sheet and it is recognised that theories such as the Kubelka-Munk assume homogeneity. However, given estimates of the mean light scattering and absorption coefficients, local homogeneity may be assumed within zones and the scattering and absorption coefficients weighted according to local density.
8. **Coupling of pore size and mass distributions.** The models for pore size distribution incorporate random and non-random cases within the same family of structures. At present, the contribution of fibres to pore size models is only to provide the boundaries to pores. By incorporating fibre width, coarseness and the number of pores per unit area, which is known analytically only for the random case, it should be possible to associate each void perimeter with a mass of fibre segments enclosing it. This links to Problem 4.

The problems presented above require primarily analytic solutions and these will typically require experimental validation. The acquisition of suitable data for such validation will itself present new problems. The solution of these problems should allow informed development of improved paper grades and of the processes by which they are formed.

ACKNOWLEDGEMENTS

The author wishes to acknowledge the substantial contribution of Dr. S.J. I'Anson in preparing Figures 3 to 7. Helpful comments on the manuscript from Dr. I'Anson and Professors C.T.J. Dodson and H.W. Kropholler are gratefully acknowledged as is the work of Dr. C.P. Wilkins in photographing the fibre suspensions presented in Figure 1.

NOMENCLATURE

Local averages of variables are denoted by placing a tilde ˜ over the variable; global averages of variables are denoted by placing a bar ¯ over the variable. *e.g*. the variable z represents sheet thickness; $\tilde{z}$ is the local average thickness, $\bar{z}$ is the global average thickness, z without a tilde or a bar is the thickness at points. The variance of local thickness at a scale of inspection x is denoted $\sigma_x^2(\tilde{z})$ and accordingly the standard deviation of thickness is denoted $\sigma_{\tilde{x}}(\tilde{z})$. The coefficient of variation of a variable is given by the ratio of it standard deviation to the mean and, for thickness, is denoted $CV_x(\tilde{z})$.

a_p	Pore area	m^2
A	Fibre aspect ratio	—
A_{floc}	Floc area	m^2
A_{insp}	Inspection area	m^2
b	Parameter of gamma distribution	m^{-1}
β	Sheet grammage	$g\ m^{-2}$
β_{fib}	Fibre grammage	$g\ m^{-2}$
c	Fibre coverage	—
C_m	Mass consistency	$kg\ m^{-3}$
C_m^{crit}	Critical mass consistency	$kg\ m^{-3}$
C_v	Volumetric consistency	—
C_v^{crit}	Critical volumetric consistency	—
$\bar{D}$	Mean disk diameter	m

D_{frac}	Fractal dimension	—
δ	Fibre coarseness	$kg\ m^{-1}$
E	Tensile stiffness	$N\ m^{-1}$
$\mathcal{E}$	Contour of equivalent pore	—
$\epsilon_1, \epsilon_2 \ldots, \epsilon_n$	Free parameters of Cosine distribution	—
ϵ_c	Free parameter of wrapped Cauchy distribution	—
ϵ_{vm}	Free parameter of von Mises distribution	—
F	Flocculation index	—
FS_{char}	Characteristic floc size	m
ϕ	Diameter of scanning aperture	m
g	free fibre length	m
$\bar{G}$	Mean disk grammage	$g\ m^{-2}$
γ	Surface tension	$N\ m^{-1}$
I	Light transmittance through a suspension	—
I_0	Light transmittance through water	—
k	Parameter of gamma distribution	—
κ	Absorption coefficient	$m^2\ kg^{-1}$
κ'	Absorption coefficient	$m^2\ g^{-1}$
$\mathcal{K}$	Weighted fractional between zones variance	—
l	Spatial wavelength	m
l_{char}	Characteristic wavelength	m
l_{macro}	characteristic length of macro-scale variation	m
l_{micro}	characteristic length of micro-scale variation	m
l_ϵ	Free parameter of elliptical distribution	—
L	Path length of light through a sample	m
L_θ	Cumulative length of fibre segments oriented between θ and $\theta + \Delta\theta$	m
$\mathcal{L}$	Cumulative length of all fibre segments	m
λ	Fibre length	m
m	Mass fraction	—
μ	Number of fibres per unit area	m^{-2}
μ_λ	Total fibre length per unit area	m^{-1}
n_{crowd}	Crowding number	—
$\overline{n^*}_{crowd}$	Crowding number considering fibre length distribution	—
n_{cross}	Number of fibre crossings per unit area	m^{-2}
n_{cross}^{MP}	Number of fibre crossings per unit area in MP sheet	m^{-2}
$n_{cross,\,fib}$	Number of fibre crossings per fibre	—

$n^{MP}_{cross,\,fib}$	Number of fibre crossings per unit fibre in MP sheet	—
$n_{cross,\,v}$	Number of fibre crossings in a volume V	—
n_{con}	Number of contacts per fibre	—
$n_{f,x}$	Formation number at zone size x	—
$n^{est}_{f,\,x}$	Estimated formation number at zone size x	—
$n_{l\theta}$	Length weighted orientation distribution	—
n_{pore}	Number of pores per unit area	—
n_v	Number of fibres in a volume V	—
n_x	Number of fibres in square zone of side x	—
υ	Spatial frequency	s^{-1}
p	Pressure	$N\,m^{-2}$
P_{cross}	Probability of intersection	—
P_{floc}	Floc perimeter	m
P_{spec}	Specific perimeter	m^{-1}
r	Distance between pairs of points	m
r_f	Fibre radius	m
r_{in}	Inscribed circle radius	m
r_p	Pore radius	m
RBA	Relative bonded area	—
$\tilde{\rho}$	Fractional between zones variance	—
ρ_w	Density of water	$kg\,m^{-3}$
ρ_{fib}	Density of dry fibre wall	$kg\,m^{-3}$
S	Bending stiffness	$N\,m$
$^\circ SR$	Schopper-Riegler wetness	$^\circ SR$
T_A	Table activity	—
θ_c	Contact angle	*rads*
ϑ	Angle between pairs of fibres	*rads*
U_x	Nonuniformity number	—
V	Volume	m^{-3}
V_a, V_b	Coefficients of variation with and without polymer	—
ψ	Orientation offset angle	*rads*
w_k	Water retention ratio	—
ω	Fibre width	m
x	Side length of square or cubic inspection zone/volume	m
z	Sheet thickness	m
z_{eff}	Effective thickness	m

REFERENCES

1. A. Swerin and L. Ödberg. Some aspects of retention aids. In **The Fundamentals of Papermaking Materials**, *Trans. XIth Fund. Res. Symp*. (C.F. Baker, ed.), pp265–350, Pira International, Leatherhead, 1997.
2. R.J. Kerekes, R.M. Soszynski and P.A. Tam Doo. The flocculation of pulp fibres. In **Papermaking Raw Materials**, *Trans. VIIIth Fund. Res. Symp*. (V. Punton, ed.), pp265–310, Mechanical Engineering Publications, London, 1985.
3. O. Kallmes, G. Bernier and M. Perez. A mechanistic theory for the load elongation properties of paper. *Pap. Tech. & Ind*. **18**(7,8,9,10), 1977.
4. K. Niskanen. Distribution of fibre orientations in paper. In **Fundamentals of Papermaking**, *Trans. IXth Fund. Res. Symp*. (C.F. Baker and V.W. Punton, eds.), pp275–308, Mechanical Engineering Publications, London, 1989.
5. K. Niskanen, I. Kajanto and P. Pakarinen. Paper Structure. Ch. 1 in **Paper Physics** (K. Niskanen, ed.). Fapet/Tappi Press, 1998.
6. J.D. Sinkey and D. Wahren. Quality comparisons of twin-wire and Fourdrinier papers. *Tappi J*. **69**(9):110–114, 1986.
7. S.G. Mason. Fibre motions and flocculation. *Tappi J*. **37**(11):494–501, 1954.
8. R.J. Kerekes and C.J. Schell. Characterisation of fibre flocculation regimes by a crowding factor. *J. Pulp Pap. Sci*. **18**(1):J32-J38, 1992.
9. R.J. Kerekes and C.J. Schell. Effects of fiber length and coarseness on pulp flocculation. *Tappi J*. **78**(2):133–139, 1995.
10. H.W. Kropholler and W.W. Sampson. The effect of fibre length distribution on suspension crowding. *In press, J. Pulp Pap. Sci., 2001.*
11. C.T.J. Dodson. The effect of fibre length distribution on formation. *J. Pulp Pap. Sci*. **18**(2):J74–76, 1992.
12. M. Deng and C.T.J. Dodson. **Paper: An Engineered Stochastic Structure**. Tappi Press, Atlanta, 1994.
13. R.E. Mark. Structure and structural anisotropy. Ch. 24 in **Handbook of Physical and Mechanical Testing of Paper and Paperboard**. (R.E. Mark, ed.), Vol II, Marcel Dekker, New York, 1984.
14. R.M. Sozynski. The apparent volumetric concentration of wood pulp fibres in suspension. *Appita J*. **42**(5):362–363, 1989.
15. D. Wahren. Proposed definitions of some basic papermaking terms. *Svensk Papperstidn*. **70**(21):725–729, 1967.
16. L. Wågberg. A device for measuring the kinetics of flocculation following polymer addition in turbulent fibre suspensions. *Svesnk Papperstidn*. **88**(6):R48-R56, 1985.
17. H. Kaji and K. Monma. Fractal analysis of flocculation in pulp suspension. In proc. *Tappi 1991 International Paper Physics Conference*, pp291–297, Kona, Hawaii. Tappi Press, Atlanta, 1991.
18. B.G. Norman, K. Moller, R. Ek and G.G. Duffy. Hydrodynamics of papermaking fibres in suspension. In **Fibre-Water Interactions In Papermaking**, *Trans. VIth Fund. Res. Symp*. (FRC, ed.), pp195–246, BPBIF, 1977.

19. L. Beghello, M. Toivakka, D. Ekland and T. Lindström. A device for measuring fibre floc sizes in highly turbulent fibre suspensions. *Nord. Pulp Pap. Res. J*. **11**(4):249–253, 1996.
20. H. Karema, M. Kataja, M. Kellomäki, J. Salmela and P. Selenius. Transient fluidisation of fibre suspensions in straight channel flow. In Proc. *Tappi 1999 International Paper Physics Conference*, pp369–379, San Diego. Tappi Press, Atlanta, 1999.
21. M. Kellomäki, H. Karema, M. Kataja, J. Salmela and P. Selenius. Fiber flocculation measurement in pipe flow by digital image analysis. In Proc. *Tappi 1999 International Paper Physics Conference*, pp461–463, San Diego. Tappi Press, Atlanta, 1999.
22. B. Norman and D. Wahren. A comprehensive method for the description of mass distribution in sheets and flocculation and turbulence in suspensions. *Svensk Papperstidn*. **75**(20):807–818, 1972.
23. I.M. Kajanto, A. Komppa and R.K. Ritala. How formation should be measured and characterised. *Nord. Pulp Pap. Res. J*. **4**(3):219–228, 1989.
24. L. Nerelius, B. Norman and D. Wahren. Measurement of flocculation characteristics by light reflection. *Tappi J*. **55**(4):574–580, 1972.
25. L. Wågberg. Adsorption of polyelectrolytes and polymer-induced flocculation of cellulosic fibres. PhD thesis, Department of Paper Technology, Royal Institute of Technology, Stockholm, Sweden, 1987.
26. L. Beghello and D. Eklund. Some mechanisms that govern flocculation. *Nord. Pulp Pap. Res. J*. **12**(2):119–123, 1997.
27. L. Beghello. Some factors that influence fibre flocculation. In Proc. Progress in Paper Physics: A Seminar. pp:A8, Vancouver, August 9–14, 1998.
28. L. Wågberg and T. Lindström. Kinetics of polymer-induced flocculation of cellulosic fibers in turbulent flow. *Coll. and Surf*. **27**(1–3):29–42, 1987.
29. A. Komppa and K. Ebeling. Correlation between the areal mass and optical densities in paper. In **The Role of Fundamental Research in Papermaking**, *Trans. VIIth Fund. Res. Symp*. (J. Brander, ed.), pp603–633, Mechanical Engineering Publications, London, 1983.
30. A. Komppa. Measurement of formation. *Pap. ja Puu* **70**(3):243–250, 1988.
31. J-P. Bernié and W.J.M. Douglas. Local grammage distribution and formation of paper by light transmission analysis. *Tappi J*. **79**(1):193–202, 1996.
32. E.S. Brazington and B. Radvan. A method of determining the substance over small areas of paper. *Tappi J*. **42**(7):545–548, 1959.
33. J.R. Parker and D. Attwood. The measurement of wire mark and the inspection of paper surfaces. *Pap. Tech*. **2**(5):T191-T198, 1961.
34. D. Attwood and J.R. Parker. Basis weight variations over small areas of paper. *Pap. Tech*. **3**(5):T133-T141, 1961.
35. T.M. Cresson, H. Tomimasu, P. Luner. Characterisation of paper formation. Part 1: sensing paper formation. *Tappi J*. **73**(7):153–159, 1990.
36. W.K. Ng. Video-beta radiography analyses of paper. BASc thesis, Pulp and Paper Centre, University of Toronto, 1993.

37. H. Tomimasu, D. Kim, M. Suk and P. Luner. Comparison of four paper imaging techniques: β-radiography, electrography, light transmission, and soft X-radiography. *Tappi J*. **74**(7):165–176, 1991.
38. H. Corte and C.T.J. Dodson. Über die Verteilung der Massendichte in Papier – Erseter teil: Theoretische Grundlagen[1]. *Das Papier* **23**(7):381–393, 1969.
39. B. Norman and D. Wahren. Mass distribution and sheet properties of paper. In **The Fundamental properties of Paper Related to its Uses**, *Trans. Vth Fund. Res. Symp*. (F. Bolam, ed.), pp7–70, BPBIF, London, 1973.
40. T. Enomae and S. Kuga. Methodology to use flat-bed image scanner for formation analysis of paper. In proc. Pre-symposium of the 10th ISWPC, Seoul, Korea, 1999: pp198–203. Korea Tappi, Seoul, 1999.
41. D.S. Keller and J.J. Pawlak. β-radiographic measurement of paper formation using a storage phosphor system. *J. Pulp Pap. Sci.,* **27**(4):117–123, 2001.
42. J.J. Pawlak and D.S. Keller. Analytical techniques for the comparison of paper formation imaging methods. *Preprint, Faculty of Paper Science and Engineering, State University of New York, 2000*.
43. P.T. Herdman and H. Corte. Comments on the distribution of mass density in paper. *Pulp Pap. Can*. **81**(10):T261-T264, 1980.
44. J.F. Waterhouse. Effect of papermaking variables on formation. *Tappi J*. **76**(9):129–134, 1993.
45. U. Wahjudi, G.G. Duffy, R.P. Kibblewhite. An evaluation of three formation testers using radiata pine and spruce kraft pulps. *Appita J*. **51**(6):423–427, 1998.
46. H. Tomimasu, P. Luner and R.B. Hanna. Rapid imaging of mass distribution in paper by electron beams. In **Fundamentals of papermaking**, *Trans. IXth Fund. Res. Symp*. (C.F. Baker and V.W. Punton, eds.), pp159–194, Mechanical Engineering Publications, London, 1989.
47. P.A. Boeckerman. Meeting the special requirements for on-line basis weight measurement of lightweight nonwoven fabrics. *Tappi J*. **75**(12):166–172, 1992.
48. T.E. Farrington. Soft X-ray imaging can be used to assess sheet formation and quality. *Tappi J*. **71**(5):140–144, 1988.
49. P.Å. Johansson. Optical homogeneity of prints. PhD thesis, Department of Pulp and Paper Chemistry and Technology, Royal Institute of Technology, Stockholm, 1999.
50. T. Cresson and P. Luner. The characterisation of paper formation. Part 2: The texture analysis of paper formation. *Tappi J*. **37**(12):175–184, 1990.
51. B.D. Jordan and N.G. Nguyen. Specific perimeter – a graininess parameter for formation and print mottle textures. *Pap. ja Puu* **68**(6–7):476–482, 1986.
52. B.D. Jordan and N.G. Nguyen. Graininess and formation ranking. *J. Pulp Pap. Sci*. **14**(2):J42-J43, 1988.
53. R.J. Trepanier, B.D. Jordan and N.G. Nguyen. Specific perimeter: a statistic for assessing formation and print quality by image analysis. *Tappi J.* **81**(10): 191–196, 1988.

[1]On the distribution of mass density in paper – part I: Theoretical basis.

54. T. Cresson and P. Luner. Description of the spatial gray level dependence method algorithm. *Tappi J*. **37**(12):220–222, 1990.
55. T. Cresson and P. Luner. The characterisation of paper formation. Part 3: The use of texture maps to describe paper formation. *Tappi J*. **38**(2):167–175, 1990.
56. R.E. Miles. Random polygons determined by random lines in a plane. *Proc. Nat. Acad. Sci. USA* **52**:901–907,1157–1160, 1964.
57. O.J. Kallmes and J.A. Ayer. Light scanning system provides qualitative formation measurement. *Pulp Pap*. **61**(4):99–105, 1987.
58. M. Bouydain, J.F. Colom and J. Pladellorens. Using wavelets to determine paper formation by light transmission analysis. *Tappi J*. **82**(7):153–158, 1999.
59. D.S. Keller, J. Lewalle and P. Luner. Analysis of paper variability using the continuous wavelet transform. *Pap. ja Puu* **81**(6):440–446, 1999.
60. D.S. Keller, J. Lewalle and P. Luner. Wavelet analysis of simulated paper formation. *Pap. ja Puu* **81**(7):499–505, 1999.
61. H. Corte. The porous structure of paper – its measurement, its importance and its modification by beating. In **Fundamentals of Papermaking Fibres**, *Trans. Ist Fund. Res. Symp*. (F. Bolam, ed.), pp301–331, Tech. Sect. BPBMA, Kenley, 1958.
62. J.P. Kettle, P. Matthews, C. Ridgway and L. Wågberg. Investigation of the pore structure of paper by novel porosimetric techniques: Application to super and soft-nip finishing. In **The Fundamentals of Papermaking Materials**, *Trans. XIth Fund. Res. Symp*. (C.F. Baker, ed.), pp1355–1393, Pira International, Leatherhead, 1997.
63. P.A. Gane, J.P. Kettle, G.P. Matthews, C.J. Ridgway. Void structure of compressible polymer spheres and consolidated calcium carbonate paper-coating formulations. *Ind. Eng. Chem. Res*. **35**(5):1753–1764, 1996.
64. T. Yamauchi and P. Kibblewhite. Pore structure of paper webs from Radiata Pine thermomechanical pulp. *Appita J*. **41**(1):37–42, 1988.
65. T. Yamauchi and P. Kibblewhite. Pore structural organisation and behaviour during the consolidation of TMP paper webs. *Appita J*. **41**(5):373–388, 1988.
66. H. Corte, Bestimmung der Porengrößyenverteilung in Papier[1]. *Das Papier* **19**(7):346–351, 1965.
67. T. Yamauchi. Measurement of paper thickness and density. *Appita J*. **40**(5):359–366, 1987.
68. W.A. Wink and G.A. Baum. A rubber platen caliper gauge – A new concept in measuring paper thickness. *Tappi J*. **66**(9):131–133, 1983.
69. V.C. Setterholm. Factors that affect the stiffness of paper. In **Fundamental properties of Paper Related to its Uses**, *Trans. Vth Fund. Res. Symp*. (ed. F. Bolam), pp253–266. BPBIF, London, 1973.
70. O. Schultz-Eklund, C. Fellers and P.-A. Johansson, Method for the local determination of the thickness and density of paper. In proc. Tappi International Paper Physics Conference, Kona, 1991: pp511–523. Tappi Press, Atlanta, 1991.
71. O. Izumi and Y. Yoshida. Development and application of a system for determin-

[1]Determination of the pore size distribution in paper.

ing paper nonuniformity. In proc. 66th Pulp and Paper Research Conference, Morioka: pp94–99. Japan Tappi, 1999.
72. R.J. Kerekes, Pulp flocculation in decaying turbulence. *J. Pulp Pap. Sci*. **9**(3):180–184, 1988.
73. H. Corte and O.J. Kallmes. Statistical geometry of a fibrous network. In **The Formation and Structure of Paper**, *Trans. IInd Fund. Res. Symp*., (F. Bolam, ed.), pp13–46, Tech. Sect. BPBMA, London, 1962.
74. T. Komori and K. Makishima. Numbers of fiber-to-fiber contacts in general fiber assemblies. *Textile Res. J*. **47**(1):13–17, 1977.
75. C.T.J. Dodson. Fiber crowding, fiber contacts, and fiber flocculation. *Tappi J*. **79**(9):211–216, 1996.
76. C.M. van Wyk. Note on the compressibility of wool. *J. Textile Inst*. **37**:T285-T292, 1946.
77. S. Toll. Packing mechanics of fiber reinforcements. *Polym. Eng. Sci*. **38**(8):1337–1350, 1998.
78. R. Meyer and D. Wahren. On the elastic properties of three-dimensional fibre networks. *Svensk Papperstidn*. **67**(10):432–436, 1964.
79. N. Pan. A modified analysis of the microstructural characteristics of general fibre assemblies. *Textile Res. J*. **63**(6):336–345, 1993.
80. T. Komori and M. Itoh. A modified theory of fiber contact in general fiber assemblies. *Textile Res. J*. **64**(9):519–528, 1994.
81. N. Pan. Fiber contact in fiber assemblies. *Textile Res. J*. **65**(10):616, 1995.
82. H. Wang and S.M. Shaler. Computer-simulated three-dimensional microstructure of wood fibre composite materials. *J. Pulp Pap. Sci*. **24**(10):314–319, 1998.
83. J.G. Parkhouse and A. Kelly. The random packing of fibres in three dimensions. *Proc. R. Soc. Lond*. A **451**:737–746, 1995.
84. K.E. Evans and A.G. Gibson. Prediction of the maximum packing fraction achievable in randomly oriented short fibre composites. *Compos. Sci. Tech*. **25**(8):149–162, 1986.
85. M. Novellani, R. Santini and L. Tadrist. Experimental study of the porosity of loose stacks of stiff cylindrical fibres: Influence of the aspect ratio of fibres. *Eur. Phys. J*. B **13**(3):571–578, 2000.
86. C.T.J. Dodson and W.W. Sampson. Spatial statistics of stochastic fibre networks. *J. Statist. Phys*. **96**(1/2):447–458, 1999.
87. V.A. Luchnikov, N.N. Medvedev, L. Oger and J.-P. Troadac. Voronoi-Delaunay analysis of voids in systems of nonspherical particles. *Phys. Rev. E*. **59**(6):7205–7212, 1999.
88. A.P. Philipse and S.G.J.M. Kluijtmans. Sphere caging by a random fibre network. *Physica A*. **274**(3–4):516–524, 1999.
89. B. Radvan, C.T.J. Dodson and C.G. Skold. Detection and cause of the layered structure of paper. In **Consolidation of the Paper Web** (ed. F. Bolam), Proceedings of the Third Fundamental Research Symposium, 1965, pp189–215. BPBMA, 1966.
90. O. Kallmes and H. Corte. The structure of paper, I. The statistical geometry of an ideal two dimensional fiber network. *Tappi J*. **43**(9):737–752, 1960. See also *Errata:* **44**(6):448, 1961.

91. C.T.J. Dodson. A contribution to the statistical rheology of bonded fibrous networks. Ph.D. thesis, Brunel University, 1969.
92. C.T.J. Dodson. Spatial variability and the theory of sampling in random fibrous networks. *J. Roy. Statist. Soc*. **B 33**(1):88–94, 1971.
93. C.T.J. Dodson. A rational approach to formation analysis and spreadsheet schema for data interpretation. *Tappi J*. **76**(5):153–156, 1993.
94. H. Corte. The structure of paper. Ch. 9 in **Handbook of Paper Science**, (H.F. Rance, ed.). Elsevier Scientific Publishing, Amsterdam, 1982.
95. H. Corte. Über die Verteilung der Massendichte in Papier – Zweiter teil: Ergebnisse an füllstoffreinen Papieren[1]. *Das Papier* **24**(5):261–264, 1970.
96. H. Corte. Statistical geometry of random fibre networks. In **Structure, Solid Mechanics and Engineering Design**, (M. Te'eni, ed.), pp341–355, Wiley Interscience, London, 1971.
97. H. Corte. Formation and the distribution of mass density in paper. *The Paper Maker* International Number: 81–85, 1971.
98. P. Luner *et al*. The relationships of wet fiber flexibility (WFF) to fiber and pulps properties. In proc. *1992 Paper Physics Seminar*, Otaniemi, Finland, 1992.
99. L. Haglund, B. Norman and D. Wahren. Mass distribution in random sheets — theoretical evaluation and comparison with real sheets. *Svensk Papperstidn*. **77**(10):362–370, 1974.
100. B. Norman. The formation of paper sheets. Chapter 6 in **Paper Structure and Properties**. (J.A. Bristow and P. Kolseth, eds.), Marcel Dekker, New York, 1986.
101. B. Norman, U. Sjödin, B. Alm, K. Björklund, F. Nilsson and J-L. Pfister. The effect of localised dewatering on paper formation. In Proc. TAPPI 1995 International Paper Physics Conference, Niagara-on-the-Lake, 1995: pp55–59. Tappi Press, Atlanta, 1995.
102. C. Schaffnit. Statistical geometry of paper: modelling fibre orientation and flocculation. Ph.D. thesis, Pulp and Paper Centre, University of Toronto, 1994.
103. W.K. Ng and C.T.J. Dodson. Rapid formation performance test. In proc. 1995 International Paper Physics Conference, Niagara-on-the-Lake. Tappi Press, Atlanta, 1995.
104. O. Kallmes, H. Corte and G. Bernier. The structure of paper, II. The statisical geometry of a multiplanar fiber network. *Tappi J*. **44**(7):519–528, 1961.
105. O. Kallmes, H. Corte and G. Bernier. The structure of paper, V. The bonding states of fibres in randomly formed papers. *Tappi J*. **46**(8):493–502, 1963.
106. O. Kallmes and G. Bernier. The structure of paper, IV. The free fiber length of a multiplanar sheet. *Tappi J*. **46**(2):108–114, 1963.
107. C.T.J. Dodson, Y. Oba and W.W. Sampson. Bivariate normal thickness-density structure in real near-planar stochastic fibre networks. *J. Statist. Phys*. **102**(1/2):345–353, 2001.
108. C.T.J. Dodson. On the distribution of pore heights in random layered fibre networks. In proceedings of this symposium, 2001.

[1]On the distribution of mass density in paper – part II: Results on unfilled papers.

109. K. Niskanen, N. Nilsen, E. Hellen and M. Alava. KCL-PAKKA: Simulation of the 3D structure of paper. In **The Fundamentals of Papermaking Materials**, *Trans. XIth Fund. Res. Symp*. (C.F. Baker, ed.), pp1273–1291, Pira International, Leatherhead, 1997.
110. E.K.O. Hellén, M.J. Alava and K.J. Niskanen. Porous structure of thick fiber webs. *J. App. Phys*. **81**(9):6425–6431, 1997.
111. R. Holmstad and Ø.W. Gregersen. Image analysis of characteristic structure elements in paper cross-sections. In proc. Progress in Paper Physics Seminar, Grenoble, Vol II:pp15–28, 2000.
112. C.T.J. Dodson, Y. Oba and W.W. Sampson. On the distributions of mass thickness and density in paper. *In press Appita J., 2001. Preprint available via www:* http://pygarg.ps.umist.ac.uk/sampson/pdf/bzc.pdf
113. H. Corte and E.H. Lloyd. Fluid flow through paper and sheet structure. In **Consolidation of the Paper Web**, *Trans. IIIrd Fund. Res. Symp*., (F. Bolam, ed.), pp981–1009, Tech. Sect. BPBMA, London, 1966. See also Discussion *ibid*.:pp1010.
114. W.C. Bliesner. A study of the porous structure of fibrous sheets using permeability techniques. *Tappi J*. **47**(7):392–400, 1964.
115. J. Castro and M. Ostoja-Starzewski. Particle sieving in a random fiber network. *Appl. Math. Modelling* **24**(8–9):523–534, 2000.
116. H.W. Piekaar and L.A. Clarenburg. Aerosol filters – Pore size distribution in fibrous filters. *Chem. Eng. Sci*. **22**:1399–1408, 1967.
117. C.T.J. Dodson and K. Fekih. The effect of fibre orientation on paper formation. *J. Pulp Pap. Sci*. **17**(6):J203-J206, 1991.
118. C. Schaffnit and C.T.J. Dodson. A new analysis of fibre orientation effects on paper formation. *Pap. ja Puu*. **76**(5):340–346, 1994.
119. T. Cresson. The sensing, analysis and simulation of paper formation. PhD thesis, State University of New York, 1982.
120. H. Praast and L. Göttsching. Local orientation of flocs in paper. In **The Fundamentals of Papermaking Materials**, *Trans. XIth Fund. Res. Symp*. (C.F. Baker, ed.), pp1293–1324, Pira International, Leatherhead, 1997.
121. R.M. Soszynski. Simulation of two-dimensional nonrandom fibre networks. Oriented rectangles with randomly distributed centroids. *J. Pulp Pap. Sci*. **20**(4):J114-J118, 1994.
122. O.J. Kallmes and G. Bernier. The structure of paper, VIII. Structure of idealized nonrandom networks. *Tappi J*. **47**(11):694–703, 1964.
123. J. Gorres, T. Cresson and P. Luner. Sheet formation from flocculated structures. *J. Pulp Pap. Sci* **15**(2):J55-J59, 1989.
124. M. Deng and C.T.J. Dodson. Random star patterns and paper formation. *Tappi J.* **77**(3):195–199, 1994.
125. P.E. Wrist. Dynamics of sheet formation on the Fourdrinier machine. In **The Formation and Structure of Paper**, *Trans IInd Fund. Res. Symp*., (F. Bolam, ed.), pp839–888, Tech. Sect. BPBMA, London, 1962.
126. R.R. Farnood, Sensing and modelling of forming and formation of paper. PhD thesis, Pulp and Paper Centre, University of Toronto, 1995.

127. R.R. Farnood, C.T.J. Dodson and S.R. Loewen. Modelling flocculation. Part I: Random disk model. *J. Pulp Pap. Sci*. **21**(10):J348-J356, 1995.
128. R.R. Farnood and C.T.J. Dodson. The similarity law of formation. In proc. *Tappi 1995 International Paper Physics Conference*, pp5–12, Niagara-on-the-Lake, Canada. Tappi Press Atlanta, 1995.
129. R.R. Farnood, N. Yan, M.T. Kortschot and C.T.J. Dodson. Modelling flocculation: A gallery of simulated flocculated papers. *Nord. Pulp Pap. Res. J*. **12**(2):86–89, 1997.
130. C.T.J. Dodson and W.W. Sampson. The effect of paper formation and grammage on its pore size distribution. *J. Pulp Pap. Sci*. **22**(5):J165-J169, 1996.
131. J. Scharcanski and C.T.J. Dodson. A new simulator for paper forming using neural networks. *Appita J*. **48**(5):347–350, 1995.
132. C.T.J. Dodson and W.W. Sampson. Modeling a class of stochastic porous media. *Appl. Math. Lett*. **10**(2):87–89, 1997.
133. W.W. Sampson. Comments on the pore radius distribution in near-planar stochastic fibre networks. *Preprint, Dept. of Paper Science, UMIST, 2000. Available via www:* http://pygarg.ps.umist.ac.uk/sampson/pdf/cvrshort.pdf
134. W.K. Ng, W.W. Sampson and C.T.J. Dodson. The evolution of a pore size distribution in paper. In proc. Progress in Paper Physics Seminar, Stockholm, June 1996.
135. P.R. Johnston. The most probable pore size distribution in fluid filter media. *J. Test. and Eval*. **11**(2):117–121, 1983.
136. P.R. Johnston. Revisiting the most probable pore size distribution in filter media. The gamma distribution. *Filtrn. and Sepn*. **35**(3):287–292, 1998.
137. J.-H. Park, S.O. Hyun, S.Y. Eim, M.K. Kim, D.H. Lee and E.H. Kim. A new evaluation system for nonwoven fabrics using image analysis technique: coverstocks, filters and interlinings. In proc. Inda-tec 1996, Crystal City, USA.
138. H.S. Kim and B. Pourdeyhimi. A note on the effect of fiber diameter, fiber crimp and fiber orientation on pore size in thin webs. *Int. Nonwovens J*. **9**(4):15–19, 2000.
139. J. Silvy. Effects of drying on web characteristics. *Pap. Tech*. **12**(5):T181-T191, 1971. See also Discussion, *ibid.*: T194-T196.
140. B. Norman. Overview of the physics of forming. In **Fundamentals of Papermaking**, *Trans. IXth Fund. Res. Symp*., (C.F. Baker, ed.), Vol III, pp73–149, Mechanical Engineering Publications, London, 1989.
141. B. Norman. Hydrodynamic developments in twin-wire forming – an overview. *Pap. ja Puu* **78**(6–7):376–381, 1996.
142. R.J. Kerekes. Perspectives on fibre flocculation in papermaking. In proc. *Tappi 1995 International Paper Physics Conference*, pp23–31, Niagara-on-the-lake, Canada. Tappi Press, Atlanta, 1995.
143. M. Steen. Concept for fiber flocculation in turbulent flow. In **Fundamentals of Papermaking**, *Trans. IXth Fund. Res. Symp*., (C.F. Baker, ed.), pp251–274, Mechanical Engineering Publications, London, 1989.
144. M. Steen. Modeling Fiber Flocculation in Turbulent Flow: Numerical Study. *Tappi J*. **74**(9):175–182, 1991.
145. M. Steen. Fibre flocculation in turbulent flow. In proc. *Flocculation Control in*

the Paper Industry, Luxembourg 10–11 March, 1992. PIRA International, Leatherhead, 1992.
146. R.R. Farnood, S.R. Loewen and C.T.J. Dodson. Estimation of intra-floc forces. *Appita J*. **47**(5):391–396, 1994.
147. S.R. Andersson, J. Ringnér and A. Rasmuson. The network strength of nonflocculated fibre suspensions. *Nord. Pulp Pap. Res. J*. **14**(1):61–70, 1999.
148. A. Chatterjee. Physico-chemical aspects of flocculation in cellulose fibre suspensions and effects on paper formation. Ph.D. thesis, Pulp and Paper Centre, University of Toronto, 1994.
149. J. Scharcanski and C.T.J. Dodson. Texture image analysis for paper anisotropy and its variability. *Appita J*. **49**(2):100–104, 1996.
150. J. Scharcanski and C.T.J. Dodson. Local spatial anisotropy and its variability. *J. Pulp Pap. Sci*. **25**(11):393–397, 1999.
151. E.R. Finger and Z.J. Majewski. Sheet formation on the Fourdrinier machine. *Tappi J*. **37**(5):216–224, 1954.
152. R.S. Seth. Fibre quality factors in papermaking – I, The importance of fibre length and strength. In proc. *Mat. Res, Symp*. **197**:125–141, 1990.
153. R.S. Seth. Fibre quality factors in papermaking – II, The importance of fibre coarseness. In proc. *Mat. Res, Symp*. 197:143–161, 1990.
154. M.J. Hourani. Fiber flocculation in pulp suspension flow. Part 1: Theoretical model. *Tappi J*. **71**(5):115–118, 1988.
155. M.J. Hourani. Fiber flocculation in pulp suspension flow. Part 2: Experimental results. *Tappi J*. **71**(6):186–189, 1988.
156. A. Raghem-Moayed and C.T.J. Dodson. Modeling stochastic fibre clumps. *App. Math. Lett*. **12**(2):7–11, 1999.
157. C.T.J. Dodson and C. Schaffnit. Flocculation and orientation effects on paper-formation statistics. *Tappi J*. **75**(1):167–171, 1992.
158. A. Kiviranta and C.T.J. Dodson. Evaluating Fourdrinier formation performance. *J. Pulp Pap. Sci*. **21**(11):J379-J383, 1995.
159. A. Kiviranta and H. Paulapuro. The role of Fourdrinier table activity in the manufacture of various paper and board grades. *Tappi J*. **75**(4):172–185, 1992.
160. J. Gorres, R. Grant, T. Cresson, and P. Luner. The effect of drainage on randomly formed papers: a simulation study. *Tappi J*. **69**(7):104–105, 1986.
161. W.W. Sampson, J. McAlpin, H.W. Kropholler and C.T.J. Dodson. Hydrodynamic smoothing in the sheet forming process. *J. Pulp Pap. Sci*. **21**(12):J422-J426, 1995.
162. B. Norman, U. Sjödin, B. Alm, K. Björklund, F. Nilsson and J.-L. Pfister. The effect of localised dewatering on paper formation. In Proc. *1995 International Paper Physics Conference*, pp55–59, Niagara-on-the-Lake, Canada. Tappi Press, Atlanta, 1995.
163. M. Lucisano and B. Norman. The forming and properties of quasi-random laboratory paper sheets. In proc. *Tappi 1999 International Paper Physics Conference*, pp331–340, San Diego. Tappi Press, Atlanta, 1999.
164. B. Radvan and A.P.J. Gatward. The formation of wet-laid webs by a foaming process. *Tappi J*. **55**(5):748–751, 1972.

APPENDIX 1: APPROXIMATE FORM OF EQUATIONS (66)

In their original form [38], Equations (66) were presented with decimal approximations for the coefficients of the functions of λ and x. These are given here with the second range, *i.e.*, for $x \le \lambda \le \sqrt{2}x$, corrected. Also, Tables 3 and 4 give the value of $\varkappa$ to three decimal places for the range of λ/x and x/λ typically used in the analysis of paper.

$$\varkappa = \begin{cases} 1 - 0.424\,\dfrac{\lambda}{x} + 0.053\,\dfrac{\lambda^2}{x^2} & \text{for } \lambda \le x \\ 1.273\left(\dfrac{x}{\lambda}\left(\log\left(\dfrac{x}{\lambda}\right) - \log\left(1 - \sqrt{1 - \dfrac{x^2}{\lambda^2}}\right)\right) + \arcsin\left(\dfrac{x}{\lambda}\right)\right. & \\ \left. + \dfrac{(\lambda^2 - x^2)^{\frac{3}{2}}}{3x\lambda^2}\right) - 0.053\,\dfrac{\lambda^2}{x^2} + 0.424\,\dfrac{x}{\lambda} - 0.106\,\dfrac{x^2}{\lambda^2} - 1.637 & \text{for } x \le \lambda \le \sqrt{2}x \\ 0.946\,\dfrac{x}{\lambda} - 0.318\,\dfrac{x^2}{\lambda} & \text{for } \lambda \ge x\sqrt{2} \end{cases}$$

Table 3 Parameter $\varkappa$ as given by Equations (66) for λ/x between 0.01 and 100.

λ/x	$\varkappa$	λ/x	$\varkappa$	λ/x	$\varkappa$	λ/x	$\varkappa$
0.01	0.996	0.1	0.958	1	0.629	10	0.092
0.02	0.992	0.2	0.917	2	0.394	20	0.047
0.03	0.987	0.3	0.877	3	0.280	30	0.031
0.04	0.983	0.4	0.839	4	0.217	40	0.024
0.05	0.979	0.5	0.801	5	0.177	50	0.019
0.06	0.975	0.6	0.764	6	0.149	60	0.016
0.07	0.971	0.7	0.729	7	0.129	70	0.014
0.08	0.966	0.8	0.694	8	0.113	80	0.012
0.09	0.962	0.9	0.661	9	0.101	90	0.011
						100	0.009

Table 4 Parameter $\varkappa$ as given by Equations (66) for x/λ between 0.01 and 100.

x/λ	$\varkappa$	x/λ	$\varkappa$	x/λ	$\varkappa$	x/λ	$\varkappa$
0.01	0.009	0.1	0.092	1	0.629	10	0.958
0.02	0.019	0.2	0.177	2	0.801	20	0.979
0.03	0.028	0.3	0.255	3	0.864	30	0.986
0.04	0.037	0.4	0.328	4	0.897	40	0.989
0.05	0.047	0.5	0.394	5	0.917	50	0.992
0.06	0.056	0.6	0.453	6	0.931	60	0.993
0.07	0.065	0.7	0.507	7	0.940	70	0.994
0.08	0.074	0.8	0.553	8	0.948	80	0.995
0.09	0.083	0.9	0.594	9	0.953	90	0.995
						100	0.996

Transcription of Discussion

THE STRUCTURAL CHARACTERISATION OF FIBRE NETWORKS IN PAPERMAKING PROCESSES – A REVIEW

W.W. Sampson
Department of Paper Science, UMIST

Dick Kerekes University of British Columbia

A very nice paper. I don't have a question, but I have a comment concerning the co-efficient .025 that you showed for the formation equations. I think we have come up with the physical explanation for this. It appears to be based on the immobilization of fibres. Fundamentally, the immobilization of fibres at papermaking crowding numbers has be extrapolate as a continuous function in the range where significant yield stress may exist. The forms of the equations for yield stress at crowding numbers well in excess of 60 are known. This is on the way to answering the question that Kit Dodson and Ari Kiviranta pointed out a number of years ago that this constant should have some physical significance.

Bill Sampson

That is very nice to hear. In particular because the coefficient you mention was determined for Fourdrinier formers and we do not have the same data for twin-wire formers. From what you say, we may expect the same coefficient for crowding number to persist for these also.

Derek Page Institute of Paper Science & Technology

There is no question that the early work of Corte and Kallmes was a revolutionary step in applying random network theory to the structure of paper. They realized quite rapidly however that they could not satisfactorily deal with the structure in the third dimension. The considered what they called a 2D sheet, which had few crossings and very few sites where three fibres

crossed. They then considered real paper as a layered array of these 2D sheets. This however was a very unsatisfactory treatment, since it did not properly account for the interaction between adjacent layers and between non-adjacent layers. It is a pity that after 40 years no one has come up with an analytical model that treats directly the whole structure, instead of dividing it into arbitrary and fictitious layers of making other assumptions that are not supported experimentally.

Karlo Niskanen faced with this problem, went the simulation route, and produced his so-called PAKKA model. He was able to simulate a sheet of regular basis weight by putting down a fibre at random on a plane surface and adding another fibre, so that when it crossed the first fibre it lay above it. He was able to incorporate the concept of flexibility by allowing the second fibre to droop down to the reference surface over a distance that depended on flexibility. He then continued to add fibres each of which could confirm to the reference surface or the fibres below it.

Maybe the analytical approach is too difficult and the simulation route would be better. I don't know where Kaarlo's simulation work has reached yet. I had some objections to some of his assumptions. But with computers getting more powerful as we speak, it should be possible now to simulate real paper, without making the unsupportable assumptions that exist in all the purely analytical models proposed to date.

Bill Sampson

There are a couple of points that arise from what you say. Firstly, regarding simulation, which I do a lot of myself, you can handle extremely complicated systems; the PAKKA model is a good example. As we have seen this week, to handle complicated systems often involves many variables and the risk there is that with a sufficient number of variables you can have almost any result that you want.

Secondly, referring to multi-planer models, and we shall hear more of these during this symposium, then it is important to be aware of the limitations of a given model. The multi-planer models of Corte and Kallmes, and the work they later carried out the Bernier, are complex. They do reveal however interesting information about, for example, the influence of fibre flexibility on the penetration of fibres between different strata of the sheet and the associated effect on bonding. When using multi-planer models, it is important to be aware that the layer is a discrete approximation for the

purposes of modelling but need not necessarily describe fully the structure of the sheet.

Kit Dodson Department of Mathematics, UMIST

Derek you should know better. After 40 years it is very difficult to get Derek to read the details. However, the fact of the matter is there are perfectly good analytic models for 3 dimensional arrangements of fibres of arbitrary shape. Bill has referred to a number of these, we have some data on the mass structure, we have data on the pore structure and on the free fibre lengths. This exists, not only that, it works, and moreover we have models which include random structures as a special case and extend into the non-random ones in 3 dimensions.